International Journal of Heat and Mass Transfer 122 (2018) 161–181

Contents lists available at ScienceDirect

International Journal of Heat and Mass Transfer

journal homepage: www.elsevier.com/locate/ijhmt

A universal wall-bubble growth model for water in component-scale high-pressure boiling systems

Janani Srree Murallidharan [a], B.V.S.S.S. Prasad [b], B.S.V. Patnaik [c,*]

[a] Department of Mechanical Engineering, Indian Institute of Technology Bombay, Mumbai 400076, India
[b] Department of Mechanical Engineering, Indian Institute of Technology Madras, Chennai 600036, India
[c] Department of Applied Mechanics, Indian Institute of Technology Madras, Chennai 600036, India

ARTICLE INFO

Article history:
Received 13 May 2017
Received in revised form 23 December 2017
Accepted 15 January 2018
Available online 2 February 2018

Keywords:
Bubble growth
High-pressure
Boiling
Phase change

ABSTRACT

Development of an accurate bubble growth model is central to the prediction of heat transfer coefficient in component scale wall-boiling formulations. The bubble growth models available in the literature are not generic enough to be applicable over a wide range of pressures. For example, pressurized water reactors operate at high pressures, where the experimental correlations are sparse. In this study, a framework for modeling wall bubble growth is developed, for water. This generalized model is synthesized in a form, which takes into account the factors that contribute to the bubble thermal layer deformation in a physically consistent way. These factors have been systematically evolved to account for a wide range of conditions (i) pressures of 1–180 bar, (ii) pool as well as flow boiling conditions, (iii) low as well as high subcooling, (iv) horizontal and vertical test section orientations, etc. Bubble growth predictions from the present model have shown very good agreement across a wide range of pressures. It was observed that, for pool boiling, the wake effect at the apex of the bubble has influenced the overall growth rate. On the contrary, for flow boiling, the flow induced distortions to the thermal layer were found to be dominant both at the base as well as the apex. In the latter case, bubble growth rate was found to be significantly dependent on the magnitude of these individual distortions.

1. Introduction

Subcooled flow boiling is a highly desired form of heat transfer in several industrial systems, since it is the most effective way to achieve high heat transfer rates at relatively low wall superheats. However, this phenomenon also has the potential to quickly transform and trigger critical safety concerns such as in the operation of high-pressure nuclear reactors. Due to the central role of subcooled flow boiling, both in efficient heat generation as well as in crisis events, there is a vast amount of literature trying to understand various facets of this phenomenon. However, the current state of understanding is far from complete, especially at high-pressure conditions, since experimental visualization techniques and measurement capabilities have considerable limitations in these conditions. Consequently, computational techniques are a sought after alternative for studying and predicting this phenomenon.

The coupled *EEMF-WHFP* mathematical framework is ideal for modeling subcooled flow boiling in component–scale systems. In this framework, *EEMF* denotes the Eulerian-Eulerian Multiphase Two-Fluid model, which is used to predict the vapour generated, within the bulk flow, in systems such as nuclear rod bundles. The vapour generation at the heated wall is modeled using the 'wall heat flux partitioning' (*WHFP*) model. Both *EEMF* and *WHFP* frameworks require inputs from a number of 'closure' models, which are in turn defined by low-pressure correlations. Since several industrial systems are operated at high pressures, model predictions based on low-pressure data often becomes questionable.

There is a real need to improve the range of applicability of the mostly low-pressure informed framework, to high pressure ranges, specifically, in the context of *WHFP* modeling. This was indeed attempted in our recent studies (see Murallidharan et al. [33,34]). The *WHFP* model essentially dictates the control and prediction of vapour, injected into the fluid domain. Hence, it is important to identify the facets of the wall boiling phenomenon that are key to achieving better prediction of high pressure subcooled flow boiling conditions and then to develop models having a wider range of applicability. The overall scope of the present work is as follows:

* Corresponding author.
E-mail address: bsvp@iitm.ac.in (B.S.V. Patnaik).

https://doi.org/10.1016/j.ijheatmasstransfer.2018.01.070
0017-9310/

Nomenclature

b_1	multiplier in ψ_1 evaluation
c	multiplier in growth constant β computation
c	specific heat of liquid (J/kg K)
f_1, f_2	multiplier
g	gravity (m/s^2)
h	latent heat of vapourisation (J/kg)
Ja	Jakob number
n_1, n_2	power constants
P	pressure (bar)
Pr	Prandtl number
T	temperature (K)
U,u	velocity (m/s)
x	variable in integral (Eq. (2))

Greek symbols

β_{IP}	growth constant
δ	natural convection thermal boundary layer
Δ	difference operator
ε	ratio of difference in density of liquid and gas to liquid density
η	diffusivity (m^2/s)
ρ	density (kg/m^3)
τ	temperature ratio
ν	kinematic viscosity (m^2/s)
ξ	ratio of phase change to latent heat in Eq. (2)
χ	multiplier in subcooling effect term
ψ_1	multiplier in wall effect parameter
ψ_{bulk}	multiplier in subcooling effect parameter
Ω	strength of superheat relative to liquid temperature in Eq. (2)
ω	gas to liquid density ratio

Subscripts

fg	fluid-gas
g	gas
IP	infinite pool of liquid
l	liquid
sat	saturated
sub	subcooled
sup	superheat

Abbreviations

AD	apex thermal layer distortion factor
BD	base thermal layer distortion factor
HS	high subcooling
HV	high velocity
LS	low subcooling
LV	low velocity
TBL/TL	thermal boundary layer/thermal layer

- A detailed study of the EEMF-*WHFP* framework to determine the most important parameters that influence the predictions under high-pressure conditions. Following the recent study of Murallidharan et al. [33], components within the *WHFP* framework requiring improvement were identified. It was concluded that the presence of the following terms aided better overall prediction of *EEMF-WHFP* model at high pressure conditions,
  i. Initial embryo size of the bubble at the time of nucleation and
  ii. bubble growth rate
- Following this, a mechanistically accurate model for initial size of the embryo formation was developed [34]. This model can account for embryo formation in both diffusive as well as stable surface nanobubble cases.
- As a continuation, of this series of work, in the present study, we propose a bubble growth model, for pressures ranging from 1 to 180 bar and for different flow conditions and bulk temperatures.
- Eventually, the embryo formation model should feed into the wall bubble growth model, which in turn should be integrated back into the EEMF-WHFP framework. Given such a holistic objective, the present study explores only the bubble growth modeling aspects of the whole.

2. Literature review

Most bubble growth models can be classified into three broad categories based on the operating conditions in which the bubble grows: (i) growth in an infinite medium, (ii) pool boiling growth and (iii) flow boiling growth. Based on this major classification, relevant background literature is categorized and elaborated in this section.

2.1. Bubble growth models in an infinite liquid medium

Bubbles growing in an infinite medium are modeled as perfect spheres growing symmetrically in a quiescent, uniformly superheated liquid medium. Although such an assumption is highly idealized, most bubble growth models follow this approach due to its simplicity. This would facilitate clear set of governing equations, with a closed-form solution to the problem on hand. Lord Rayleigh was one of the first to address a problem description of this nature. He modeled the variation of pressure inside a bubble cavity as it collapses [39]. This was achieved by equating the kinetic energy required for the motion of the inner boundary of the cavity from an initial size of radius r_o to a final radius r to the work done in forming the cavity. Plesset and Zwick [35] were the first to propose a heat-transfer/vaporization based 'growth' model for the bubble. Here, they modified the original equation of Rayleigh [39] to account for the cooling effect caused by evaporation at the bubble interface. The growth is assumed to occur due to conduction heat transfer across the thermal boundary layer between the superheated bulk fluid and the bubble interface. Thus, the bubble growth is limited by the rate at which the heat of evaporation is supplied to the interface (heat diffusion controlled). Forster and Zuber [16] also developed a growth formulation that is similar to the model of Plesset and Zwick [35]. Though their equations handle the temperature condition for the asymptotic growth differently, there is physical equivalence [52]. Both these models are, however, approximate [52] and require the input of tuning constants. Scriven [42], unlike the previous models, presents an exact solution for bubble growth. He included in his model the effect of radial convection on growth (due to unequal phase densities) and also defined the bubble growth constant 'β_{IP}' in terms of phenomenological parameters. However, his formulation for the growth constant 'β_{IP}'is complex and the alternate (approximate) versions suggested in his work are accurate, only for a specific portion of the bubble growth curve [42]. Board and Duffey [6] proposed a spherical bubble growth model in a uniformly superheated liquid by proposing a theory based on thermal equilibrium at the bubble interface. This theory was used for predicting bubble growth for cases, where different fluids having similar growth rates are involved. Their model predicted growth of sodium vapour bubbles in water reasonably well. Theofanous et al. [47]

modeled bubble growth by incorporating the non-equilibrium effects near the liquid–vapour bubble interface and accounted for variable vapour density. This model was also found to depend largely on the vaporization coefficient, a tuning parameter [47].

The validation for most of these infinite medium bubble growth models was carried out against bubbles rising in superheated liquid or against bubbles growing at a heated wall. Plesset and Zwick [35] validated their model, for water, by comparing it with the near-atmospheric pressure experiments of bubbles slowly rising in a uniformly heated liquid [13]. Scriven's [42] model is validated for near-atmospheric pressure data of Dergarabedian [13] and Faneuff et al. [15]. While Dergarabadian's experiment accommodates freely rising bubbles, the experimental data of Faneuff et al. [15] accounted for bubbles growing on a heated surface. Scriven [42] compared his model with that of Plesset and Zwick [35] and Forster and Zuber [16] and concluded that, the latter two are only valid for a restricted range of pressures and wall superheats. Kosky [22] performed bubble growth experiments with uniformly superheated water for pressures varying from 0.5 to 1.2 atm. He found that, Plesset and Zwick's model was able to capture the asymptotic part of the bubble growth accurately. Van Stralen [52] compared the theories of Plesset and Zwick, Forster and Zuber and Scriven and showed that Scriven's and Plesset and Zwick's model converge for relatively large superheats. Van Stralen [52] also compared the models against experiments for both adhering and released bubbles on a platinum wire (1967), and concluded that Scriven's model provided good predictions. It is to be noted here that, most of these models were validated only at or near atmospheric pressures.

A few studies focused on studying the performance of these infinite medium models at other operating conditions and tried to reconcile the experimental observations with their formulations. Cole and Shulman (1966) compared predictions of various bubble growth models for high Jakob numbers and concluded that, the infinite bubble growth formulation tend to overpredict. This overprediction was attributed to the model used for the growth constant and not the shape of the growth curve. In most studies the growth curve was found to vary as $(growth\ time)^{\frac{1}{2}}$ i.e. $t^{\frac{1}{2}}$. Additionally, Cole and Shulman (1966) recommend the use of $(\Delta T_{sup}/2)$ instead of ΔT_{sup} for Jakob numbers < 100 where ΔT_{sup} represents the wall superheat. However, Saddy and Jameson [40] observed bubble growth varying as $t^{\frac{3}{4}}$ at similar atmospheric conditions. Similarly, Darby [12] conducted a photographic study of bubble growth in superheated water and Freon (R113) and observed that the radius of the bubble varied as $t^{\frac{2}{3}}$. From the above literature on infinite medium bubble growth models, discrepancies in both the structure as well as the value of the growth constant can be observed.

2.2. Models for pool boiling

A number of physically realistic formulations, which model bubble growth under pool boiling conditions were proposed. Cole and Shulman [9] tested the predictions of some of the initial wall-bubble growth models such as Zuber [60] against experiments and concluded that, these models are less accurate than the infinite medium bubble growth formulations (Eq. (12) in [9]). Cooper and Lloyd [11] conducted pool boiling experiments at low pressures to study the effect of microlayer evaporation in bubble growth. They concluded that the rate of evaporation of the microlayer is of the same order, as the rate at which bubble grows. They have proposed an analytical expression with suitable tuning constants to fit their experimental data. Mikic et al. [29] have developed one of the most prominent wall-bubble growth models which is valid for both inertia and heat-transfer controlled regimes. They modeled growth as occurring in a non-uniform temperature distribution. Biasi et al. [5] have developed a model for bubble growth in linearly varying temperature profiles and compared them to Cole and Shulman's [9] experiments for low pressures of water. Their model overpredicted the experiments and it was concluded that, this was due to the model's assumption that the bubble was hemispherical, whilst growing at the wall. Van Stralen et al. [53] proposed a bubble growth model, which included the effects of relaxation layer and microlayer. The formulation is however complex and they have not validated against any experimental data. Dwyer [14] developed a bubble growth model specifically for liquid metals in which he accounted for the heat transfer through the solid surface as well as a hemispherical bubble interface. Though his model is restricted to liquid metals, it was predicted that, the heat transfer rates from the surface as well as the hemispherical interface are comparable. Miyatake et al. [26] have improved the model of Mikic et al. [29] by incorporating acceleration effects and variable fluid properties into the wall bubble growth. Recently, Lesage et al. [24] developed a bubble growth and detachment model for adiabatic, non-boiling conditions based on only geometric considerations of the bubble. This method was further extended in Lesage et al. [25] to model nucleate boiling bubble growth from artificial cavities in low saturation temperature cases of n-Pentane vapour bubbles. Similar to the infinite medium growth formulations, pool boiling models have been validated mostly against low pressure experiments and therefore, have a limited operating range. Very few studies have been reported in the open literature for high pressure range. Sakashita [41] who performed saturated boiling experiments of water at ~45 bar and proposed an empirical bubble growth model is the most prominent among them.

A separate class of bubble growth models for pool boiling employed finite difference based techniques to capture the physics. Griffith [17] performed computations to study the effect of the wall on a growing bubble. His method required several input parameters from experiments, most important amongst them being the thickness of the thermal boundary layer. Han and Griffith [18] improved this model by including several additional tuning factors such as curvature factor, shape factor, base factor, and volume factor. Their validation was predominantly against atmospheric bubble growth experiments. Mei et al. [27] performed finite difference based calculations and identified four parameters governing bubble growth: Jakob number, Fourier number, solid–liquid thermal conductivity ratio and solid–liquid thermal diffusivity ratio. They have also accounted for the unsteady energy transfer from the microlayer. Nevertheless the validation is limited to near atmospheric conditions. Lee and Merte [23] have used a similar finite difference based modeling of bubble growth in sub-atmospheric and atmospheric conditions. Comparisons were made with infinite bubble growth models of Scriven [42], Plesset and Zwick [35] as well as wall growth model of Mikic et al. [29]. However, the improvements achieved were not very significant.

2.3. Models for flow boiling

Under flow boiling conditions, very few wall bubble growth models are available in the literature. Unal [48] proposed a semi empirical correlation for bubble growth in subcooled flow boiling conditions of water up to 17.7 MPa. According to this study the bubble growth depends on liquid thermal conductivity and a pressure dependent constant. Yun et al. [59] have modeled bubble growth through a superimposition of, superheating as well as subcooling effects. The model of Colombo and Fairweather [10] accounts for three factors: microlayer, superheated liquid layer and the subcooling effect. Raj et al. [37] have proposed a bubble growth model based on energy conservation principles applied to

a bubble growing at the nucleation site. They have accounted for heat transfer from evaporative and superheated microlayer as well as condensation at the vapour interface. However, these and similar such studies are mostly modeled and validated for low pressure conditions.

2.4. Heat transfer mechanisms during bubble growth

Different heat transfer mechanisms involved during the bubble growth process have been identified through several experimental and computational studies. Most studies have identified the microlayer evaporation as the dominant mode of heat transfer. In their early studies, Judd and Hwang [19] have observed that, the microlayer evaporation is the most important contributor to the total heat transfer. Ammermann et al. [2] have concluded that evaporation is the most dominant phenomenon, while Bae et al. [3] have specifically identified evaporation near the contact line to be most significant. In the computational study of Stephan and Fuchs [45], the strongest cooling of the heater was observed adjacent to the moving micro region. Here, the temperature dip was measured to be around 0.5–5 °C. Some recent experimental studies with highly advanced instrumentation were able to shed more light on bubble growth heat transfer. For example, Jung and Kim [20] could measure the actual dimensions of the microlayer as a function of the growing bubble and were able to quantify the actual heat transfer that the microlayer is responsible for. From their study of saturated pool boiling in water, Yabuki and Nakabeppu [56] have shown that the contribution of microlayer evaporation to bubble growth is about 50%. This study was further extended to subcooled boiling conditions of water [58], and herein it was observed that the microlayer evaporation continued to ensure a significant contribution to the wall heat transfer. Detailed visualization of the microlayer structure has been carried out by Utaka et al. [49,50], and Chen et al. [8]. In Utaka et al. [49,50], the microlayer structures formed during boiling of water and ethanol were characterized. It was observed that the initial microlayer thickness increased linearly with distance from the nucleation site. Chen et al. [8] as a continuation of this investigation observed that there are two distinct shapes for the microlayer formed (for water): (a) a linearly varying structure during expanding stage of microlayer, and (b) a 'bent' shape after the microlayer reaches the maximum radius. Utaka et al. [49] also found that the microlayer thickness in ethanol was twice as thick as in water [49]. However, the microlayer evaporation for ethanol was found to be approximately only one third of that for water [50]. This was attributed to the lower thermal conductivity and thicker microlayer for ethanol. It is important to note here that ethanol has low vaporization heat whereas water has a higher vaporization heat. Hence, water being a liquid having higher vaporization heat ensures higher microlayer evaporation heat transfer. However, the percentage contribution to the total bubble volume through microlayer evaporation is comparable for both ethanol and water. It increases from 20% to 70% for a superheat increase from 10 K to 40 K (Fig. 20 in [50]).

Some studies have also analyzed the period over which the bubble grows and as to when maximum heat transfer is achieved, the response of the heater, the surrounding liquid, etc. Bae et al. [3] state that the heat transfer is highest during the departure process i.e. from the time the contact line reaches the maximum radial position to the departure time. Ammermann et al. [2] identified micro-convection to be the mechanism responsible for entrainment of superheat liquid in the trailing region of the rising bubble. More recently, Yabuki et al. [55] were able to capture this entrainment more clearly in their experiments. Stephan and Fuchs [45] in their numerical study showed that the bubble growth and detachment period consumes more heat (through evaporation) than heat supplied to the overall system. Thus, as a consequence, the wall and liquid thermal boundary layer cool down. The vice versa occurs during the waiting period. Yabuki et al. [55] were also able to observe based on the behavior of the thermal boundary layer, that condensation occurs in some cases when the bulk is subcooled. In fact it was observed in their study using water that the condensation heat transfer observed at the bubble apex was comparable to the microlayer evaporation [57]. Moghaddam and Kiger [30] through their experiments identified three different mechanisms of heat transfer (1) microlayer evaporation (2) transient conduction due to rewetting (3) micro-convection in the region external to the bubble/surface contact area. In fact, Stephan and Fuchs [45], summarizes that, the interaction between, microscale evaporation, macroscale transient heat flow in the wall, and the heat transfer in the thermal boundary layer, is a key aspect in bubble growth. Further analysis on these key interaction aspects using high-resolution imaging techniques would be most beneficial.

From the literature discussion above, the following conclusions can be drawn:

- Evaporation, both from the microlayer and the surrounding fluid, is important. Microlayer evaporation was identified as dominant in several studies.
- Heat transfer in the receding phase of the bubble growth is significant.
- Due to bubble growth, there is a cooling of both the heater and the thermal boundary layer.
- Rewetting of the heater surface was found to be a significant mode of heat transfer.
- Superheated liquid has been observed to be dragged-up in the trail of a rising bubble. Hence one can assume that cooler liquid will be convected to occupy the near wall region vacated by this liquid, and this in turn will influence the growth of the subsequent bubble.

The bubble growth model will be developed taking into account these observations.

2.5. Present study in perspective

From the literature on bubble growth models, it can be observed that, most of the infinite medium bubble growth models are only approximate. Moreover, they are mostly developed for near atmospheric pressure conditions, which restricts their range of applicability. Amongst them, Scriven's [42] infinite bubble growth model is found to be more mechanistic with reasonably good predictions when tested for atmospheric pressures [51,52,42]. Following this, the literature on pool boiling bubble growth studies suggest that, wall effects such as (a) transitioning from inertia to heat transfer controlled growth [29] (b) wall-normal temperature gradation [29,26] and (c) microlayer effects [53] need to be accounted, for a better bubble growth rate predictions at the wall. However, the studies that have implemented these formulations largely cater to only near-atmospheric pressures. Moreover, when compared to infinite medium bubble growth models, these pool boiling models are less accurate, have a limited range of applicability, too complex to implement etc**.** Flow boiling bubble growth models attempt to capture different aspects of the flow phenomena such as, subcooling and superheating effect by the principle of superposition [58,10]. However, these models are tuned and tested for near atmospheric pressures only. It may be pertinent to note that, most of the subcooled flow boiling studies use pool boiling/infinite medium bubble growth models for their predictions due to its ease of implementation (Yeoh et al., [58]).

Unal [48] proposed a model to predict bubble growth up to 177 bar. Though this model has a similar pressure range as our proposed model, there are some significant differences compared to

their formulation. Unal's [48] model essentially divides the bubble growth process into two regions: (i) the growth/evaporation into the bubble occurring from a thin liquid layer under the bubble (ii) Condensation occurring at the top. However, at high pressures, the bubbles are likely to be extremely small and submerged inside the superheated thermal boundary layer near the wall. Hence, restricting evaporation only to the liquid layer underneath the bubble would be inaccurate. To realistically capture the bubble growth phenomena, the proposed model accounts for evaporation over the entire region of the bubble. The model of Unal [48] restricts condensation to the top of the bubble. However, in reality, when there is high velocity, there is a chance of liquid penetration near the upstream base of the bubble. This can locally cause a decrease in the growth, which is captured through the present model. Moreover, Unal's [48] model limits the use of the velocity effect to the condensation term, which is not always the case in reality. Increased velocity can at times result in making the boundary layer thinner for the same temperature difference and thereby increases the strength of heat transfer and growth. The velocity effect in the present model is not restricted to condensation. Hence, the present model formulates the bubble growth in a much more physically realistic way than Unal's [48] model.

The motivation to develop the present wall bubble growth model comes from the need to address some of the important lacunae that have been identified. From the literature review presented in Section 2, it can be noticed that, not a single model is applicable for both pool and flow boiling conditions, as well as for superheated, saturated and subcooled conditions. Although such generalized models have been attempted, they are confined to the atmospheric pressure conditions only. Hence, it is desirable to have a single generalized model that can predict across a wide range of pressures, in particular, for high pressure boiling systems. Additionally, it has been identified from the review that, all the key factors contributing to bubble growth can be classified into three main categories (a) pressure effect (b) flow effect and (c) subcooling effect. A wall bubble growth model accounting for all the aforementioned effects and with a wide applicability range is developed in this paper. In Section 3, the framework for the development of this model is presented. Section 4 presents the bubble growth rate predictions under pool boiling as well as flow boiling conditions. The paper ends with a brief summary in Section 5.

3. Formulation for the wall-bubble growth model

The present study proposes a generalized wall-bubble growth model, which is applicable over a wide range of operating conditions. From the literature review, it was identified that Scriven's [42] infinite medium bubble growth constant is both mechanistic and accurate. Therefore, we propose a simplified formulation based on Scriven's 'β_{IP}' formulation. Additionally, it was noticed that, wall effects need to be appropriately modeled to achieve an accurate prediction. Hence, wall asymmetricity, subcooling and flow effect are systematically incorporated into the present modeling framework.

3.1. Overview of the framework

3.1.1. Bubble growth physics

- *Growth of the bubble when in a superheated infinite liquid medium:* The bubble will grow based on the rate at which it receives heat at the interface, where phase change is taking place. In the initial stages, the bubble interface has complete and immediate access to superheated liquid and hence, the bubble grows at a faster rate. Here, the growth rate is limited by the inertia of the surrounding liquid, and the growth process is known as the inertia-controlled growth. Subsequently, the temperature immediately adjacent to the interface drops and a thermal boundary layer is formed whose temperature varies from the saturation temperature at the interface and the superheated bulk medium (Fig.1a). The transfer of heat across the thermal boundary layer is modeled as conduction heat transfer and is known as heat diffusion controlled growth. Scriven's [42] calculated this heat diffusion controlled heat transfer.
  In our model, one component uses Scriven's formulation and calculates the heat diffusion controlled infinite bubble growth (discussed in detail in Section 3.1.2). It is important to point out that, this component accounts for the growth when the bubble is completely surrounded by a medium that is superheated.
- *Growth of bubble at the wall:* When a bubble is at the wall, it is not completely surrounded by superheated medium as in the previous case. There is a superheated wall on one side, and also some region of superheated water near the wall. But, there is also a possibility that a portion of the bubble interface will be exposed to liquid at a temperature lesser than the superheat. The extent of this exposure depends on the operating conditions maintained by the experiment i.e. if the bulk is subcooled, saturated, or has a flow, etc.
  This non-uniformity in temperature will be further amplified by various heat transfer mechanisms occurring during the bubble growth process. The reason for different heat transfer mechanisms to exist is mainly due to the surface tension, and the contact angle effect, of the interface at the wall. The contact angle effect influences the movement of the interface at the wall during the advancing-contact-angle phase of the bubble growth, as well as during the receding-contact-angle phase. The two major effects from the contact effect is (a) the formation of microlayer in the initial parts of bubble growth and (b) the role it plays in the departure of the bubble from the wall. Based on the conclusions drawn from the literature study, it can be seen that the thermal boundary layer will be distorted by the various heat transfer mechanisms. The effect for these mechanisms, which are essentially due to the presence of the wall, has been combined in the present model as the 'wall-effect multiplier'. Since these mechanisms, as observed in the experiments, result in some form of cooling of the heater and the near-wall fluid, the Jakob number Ja_{sat} is defined based on the saturation temperature and not the superheat temperature.

3.1.2. The framework

It is well known that, the thermal layer (TL) surrounding the bubble interface, not only influences its shape and size, but drives the bubble growth as well. Obviously, the distortion of the thermal boundary layer as mentioned in the previous section will influence the bubble growth. Hence, the present study incorporates suitable correction factors to implement these phenomenological features into the original 'infinite bubble growth' formulation. Hence, in the proposed bubble growth model, three main factors (see Fig. 1) have been identified viz.,

i. *Infinite bubble growth component:* This refers to the bubble growth in an infinite medium i.e. when the TL around the bubble interface (assumed to vary between the superheated bulk and the saturation temperature at the bubble interface) is circular and is of uniform thickness as shown in Fig. 1(a). Note that within the TL, the temperature varies between the saturated bubble interface and the superheated liquid bulk.

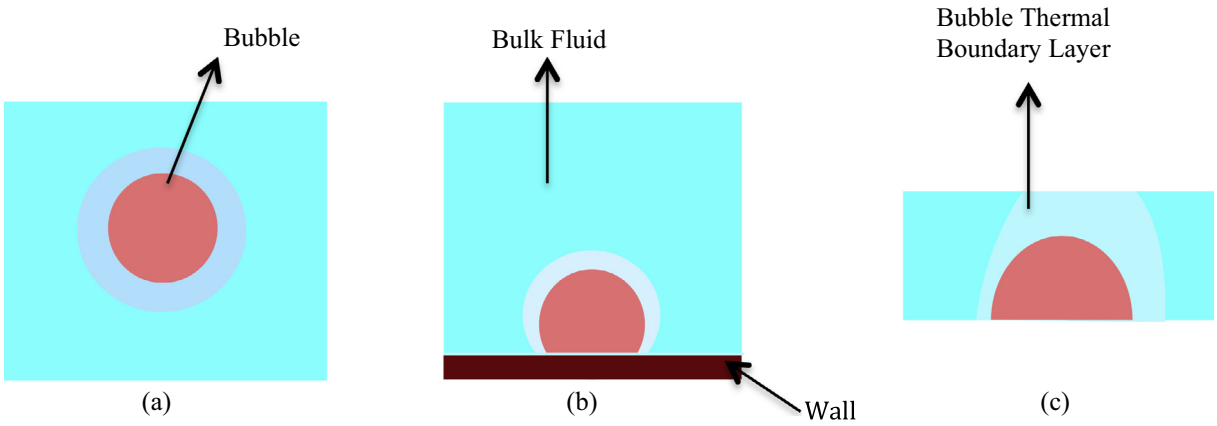

Fig. 1. Thermal boundary layer around a bubble (a) idealized case in an infinite superheated medium (b) bubble near a wall (c) subcooling effect on the apex of the wall bubble.

ii. *Wall effect multiplier:* For a bubble growing at the wall, certain asymmetricity exists in the shape and thickness of the TL near the wall-bubble contact line as shown in Fig. 1(b). The wall effect multiplier captures the effect of this distortion, on the bubble growth rate.
iii. *Bulk effect multiplier:* A bubble growing at the wall is not only influenced by the presence of the wall and its superheat, but also the fluid conditions. For example, when a bubble comes in contact with the subcooled bulk, there is either a decrease in its growth rate or a decrease in bubble size due to condensation at the apex. This is due to a change in the thickness of the TL at the apex of the bubble as shown in Fig. 1(c). This TL distortion is captured through the bulk effect multiplier.

In this formulation, system pressure, bulk subcooling and flow velocity are considered to have a significant impact on bubble growth. These aspects were experimentally studied by Sugrue [46], with the aid of high-speed imaging for different orientation angles, mass flux, pressures and subcooling. Her study measured the variation in bubble departure diameter, over a range of operating conditions. It was shown that, the bubble growth rate decreases with increase in flow velocity. Moreover, there are several Reynolds number based formulations, which employ force balancing based equations for the bubble departure diameter (Sugrue, [46]). These predominantly empirical expressions also indicate that the bubble size will decrease with increase in velocity for most cases. This can be attributed to the improved heat removal due to increased convection and an overall decrease in the superheat of the system. It was also observed from Sugrue's experiments that the bubble growth increases with decrease in subcooling. However, Sugrue [46] states that the subcooling effect is not dominant in cases where the bubble size is small in comparison to the thermal boundary layer. This implies that, the farther the bubble is from the bulk liquid, the slower the condensation on the bubble interface. The decreased condensation effect leads to an improved bubble growth rate. Sugrue [46] also observed that bubble growth increases with decrease in pressure, which she substantiates using an ideal gas law where, the pressure is inversely proportional to the volume. Thus, the size of the bubble will vary inversely to the cube root of pressure. All these experimental observations are translated in our phenomenological formulation for bubble growth, which is described in Section 3.2.

3.2. Phenomenological formulation

In view of the framework presented in Section 3.1.2, the radius of the bubble growing at the wall is formulated as,

$$R(t) = \underbrace{2\beta_{IP}\sqrt{\eta t}}_{IBG}\ \underbrace{(Ja_{sat}\Psi_1 f_1)}_{WEM}\ \underbrace{\Psi_{bulk}}_{BEM} \tag{1}$$

We can notice that, the framework comprises of three distinct components viz., Infinite bubble growth (IBG), Wall Effect Multiplier (WEM) and Bulk Effect Multiplier (BEM), which are identified in the equation.

3.2.1. Infinite Bubble Growth (IBG) component ($2\beta_{IP}\sqrt{\eta t}$)

This term is similar to the standard framework of bubble growth models, and it is retained here for the infinite bubble growth component. Here, β_{IP} refers to the growth constant which is based on Scriven [42] model. In the literature review section, Scriven's [42] bubble growth constant was identified as having a mechanistic formulation with a good predictive capability. However, the formulation is complex and not suitable for easy implementation into a bubble growth model. Hence, a simple formulation is highly desirable for implementing into component scale wall boiling models. This is because, the coupled *EEMF-WHFP* computational fluid dynamics (CFD) solvers tend to diverge when coupled with models that require complex mathematical solution strategies. This is perhaps due to lower order accuracies and numerical errors of various constituent methods in CFD. Since, the goal here is to develop a bubble growth model for an accurate boiling prediction in component-scale boiling studies, a simple form of the model would help users to easily implement and simulate wall boiling in a coupled *EEMF-WHFP* framework. Hence, a simplified formulation of the Scriven's β_{IP} is developed.

Scriven [42] originally proposed a model for the bubble growth constant as follows:

$$\frac{\Omega}{\xi + \omega(\Omega v)} = \phi(\varepsilon, \beta_{IP}) \equiv 2\beta_{IP}^3 e^{\left(\beta_{IP}^2 e^{\left(\beta_{IP}^2 + 2\varepsilon\beta_{IP}^2\right)}\right)} \int_{\beta_{IP}}^{\infty} x^{-2} e^{\left(-x^2 - 2\varepsilon\beta_{IP}^3 x^{-1}\right)} dx \tag{2}$$

where

$\xi = \frac{\rho_g h_{fg}}{\rho_l c_l (\Delta T_{sup} + T_{sat})}$	–	The fraction of heat required for phase change to the sensible heat required to maintain the liquid at a temperature above the saturation temperature (i.e. at superheat temperature)
$\Delta T_{sup} = T_{liq} - T_{sat}$	–	Difference between the superheated liquid temperature and the saturation temperature
$\Omega = \frac{\Delta T_{sup}}{\Delta T_{sup} + T_{sat}}$	–	Strength of the superheat relative to the liquid temperature.
$\nu = \frac{c_l - c_g}{c_l}$	–	Change in specific heat due to phase change relative to the liquid specific heat
$\omega = \frac{\rho_g}{\rho_l}$, $\varepsilon = 1 - \omega$	–	ω denotes the ratio of gas to liquid density

In Eq. (2), x is a mathematical construct and serves as an independent variable for integration. In the present case the limits of the integration show that it represents the growth factor of a bubble in an infinite pool of liquid.

According to Scriven's [42] model, the bubble growth constant is dependent on parameters relating to the heat capacity of the system and the fluid properties. Firstly, Boiling studies relevant to the present work do not usually see superheats greater than 100. Hence, from the plots of Scriven [42] one can say that among the fluid property terms, the variation of density with pressure appears to influence the bubble growth process more than the variation of specific heat. Hence in the present study, the influence of specific heat is not included in the bubble growth variation and includes the density ratio (ω) as a parameter in the β_{IP} formulation. Secondly, Scriven's model has two separate terms (ξ and Ω) to denote heat capacity of the system. In the present study, both the liquid and vapour in the system is considered to be at least at the saturation temperature. Hence, any heat input, which is required, would be used to maintain the system at a specified superheat in order to facilitate phase change. Hence, parameterizing the fraction of heat required for phase change to that of the sensible heat required is sufficient to characterize the problem. Consequently, instead of using two separate terms, ξ and Ω, to denote heat capacity, Jakob number *(Ja)* is used in the formulation. Hence, the present β_{IP} formulation expresses the growth constant purely in term of *Ja* and ω.

To start with, Scriven's formulation was first implemented and calculations were performed for a pressure range of 1–180 bar and

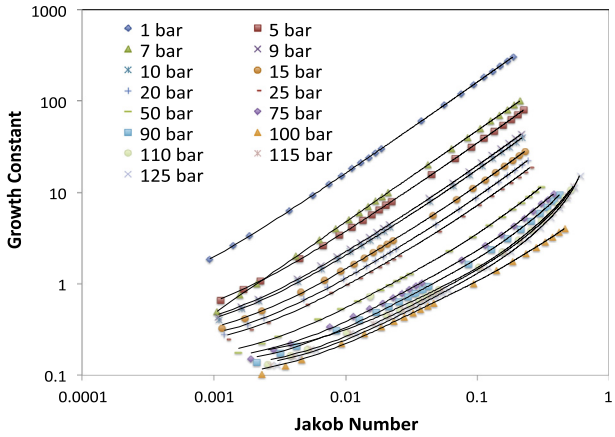

Fig. 2. Variation of growth constant (β_{IP}) against Jakob Number (*Ja*) for P = 1–125 bar of water.

for several values of superheat. The variation of growth constant against *Ja* and ω are plotted in Figs. 2 and 3, which depict β_{IP} vs. *Ja* for P < 125 bar, and P > 125 bar respectively. The curves for the different pressures are denoted by the density ratio of the liquid to vapour at that specific pressure (ω). From the best fit correlations, a single trend can be noticed for P < 125 bar, while two distinct trends are observed for P > 125 bar. The latter (Fig. 3) denotes two separate fitting correlations.

The expression for β_{IP} developed for P < 125 bar is of the form

$$\beta_{IP} = -c_1 Ja^6 + c_2 Ja^5 - c_3 Ja^4 + c_4 Ja^3 - c_5 Ja^2 + c_6 Ja + c_7 \quad (3)$$

For P > 125 bar and Ja < 0.5 it is

$$\beta_{IP} = c_1 Ja^{c_2} \quad (4)$$

and for P > 125 bar and Ja > 0.5 it is

$$\beta_{IP} = c_1 \ln(Ja) + c_2 \quad (5)$$

Following this, the variation of the coefficients in the Eqs. (3)–(5) against ω are plotted in Fig. 4 (P < 125 bar) and Fig. 5 (P > 125 bar). It is observed that the trend of coefficients for P < 5 bar differs from those in P = 5–125 bar. The present formulation simplifies the β_{IP} calculations and the coefficients that have been developed are summarized in Table 1. It is to be noted here that the Jakob number used in the calculation of the growth rate is computed using the wall superheat. This implies that the bubble growth component generates the ideal growth, as if the bubble is surrounded by bulk fluid, which is at a temperature equal to the wall superheat temperature.

3.2.2. Wall effect multiplier-($Ja_{sat}\psi_1 f_1$)

For a bubble growing at the wall, a portion of the bubble interface is in contact with the wall. In the region adjacent to the bubble-wall contact line, the thermal layer is distorted (Fig. 6), compared to an ideal TL in an infinite medium (Fig. 1(a)). Fig. 6 is a qualitative and a highly idealized illustration of how the temperature field would interact with a growing bubble at the wall, and the resulting distorted zone governs the size and shape of the TL region. This TL distortion will cause a deviation in bubble growth, which is captured through the wall effect multiplier.

Factors that influence the growth of the near-wall bubble interface are the thickness of the TL and shape of the distorted region, the temperature gradation, length of the interface in contact with the wall etc. Since bubble growth phenomenon is highly coupled and complex, it is not possible to separately quantify each of these factors. To this end, the above aspects are modeled as follows:

- Ja_{sat}(*Thermal component*): Firstly, a multiplier is included to modify growth with reference to the infinite medium, and this is expressed in terms of the saturated Jakob number (Ja_{sat}). This Ja_{sat} represents the ratio of the sensible heat required to maintain the fluid at saturation temperature to the heat required for phase change. The saturation temperature is used in the wall effect multiplier formulation to take into consideration, the effect the presence of a wall has, on the idealized growth of a bubble in an infinite superheated medium. Fig. 6. This term also accounts for the microlayer heat transfer. Just prior to and at the time of nucleation, the wall is at superheat temperature. However, as soon as an embryo nucleates and grows, a microlayer is formed. Here, it is seen that the upper boundary will be the liquid-vapour interface, which is at the saturation temperature. The dimension of the microlayer is extremely small in comparison to the bubble size. Hence, for the purposes of the present study, resolving the microlayer and solving the heat transfer across it, is not an efficient technique. However, the microlayer does contribute significantly to the growth process. Hence, we

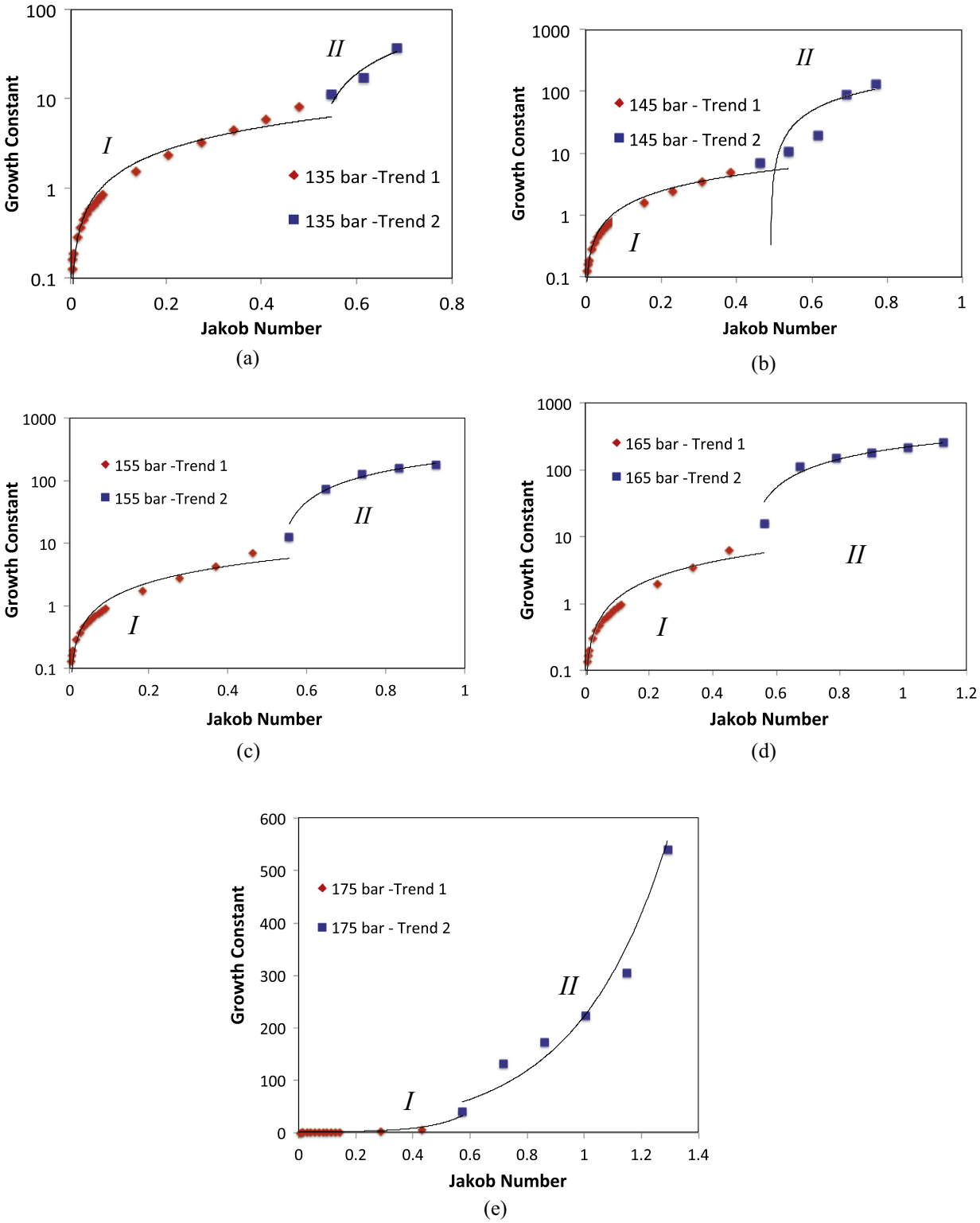

Fig. 3. Variation of growth constant (β_{IP}) against Jakob Number (Ja) at higher pressure (P) for water. (a) P = 135 bar I: $\beta_{IP} = 10.571Ja^{0.8476}$ II: $\beta_{IP} = 112.49\ln(Ja) + 76.716$. (b) P = 145 bar I: $\beta_{IP} = 9.687Ja^{0.8509}$ II: $\beta_{IP} = 245.14\ln(Ja) + 173.89$. (c) P = 155 bar I: $\beta_{IP} = 9.5982Ja^{0.8784}$ II: $\beta_{IP} = 330.58\ln(Ja) + 214.4$. (d) P = 165 bar I: $\beta_{IP} = 9.6171Ja^{0.9116}$ II: $\beta_{IP} = 317.07\ln(Ja) + 214.91$. (e) P = 175 bar I: $\beta_{IP} = 0.2557e^{8.3977Ja}$ II: $\beta_{IP} = 9.3736e^{3.1611Ja}$.

have attempted to include its contribution by estimating the likely effect that the presence of the microlayer would have on the thermal boundary layer near the wall. Since (a) the microlayer induces increased heat transfer, which results in local cooling of the heater temperature (b) the vaporization at the interface induces a small amount of flow into the micro-

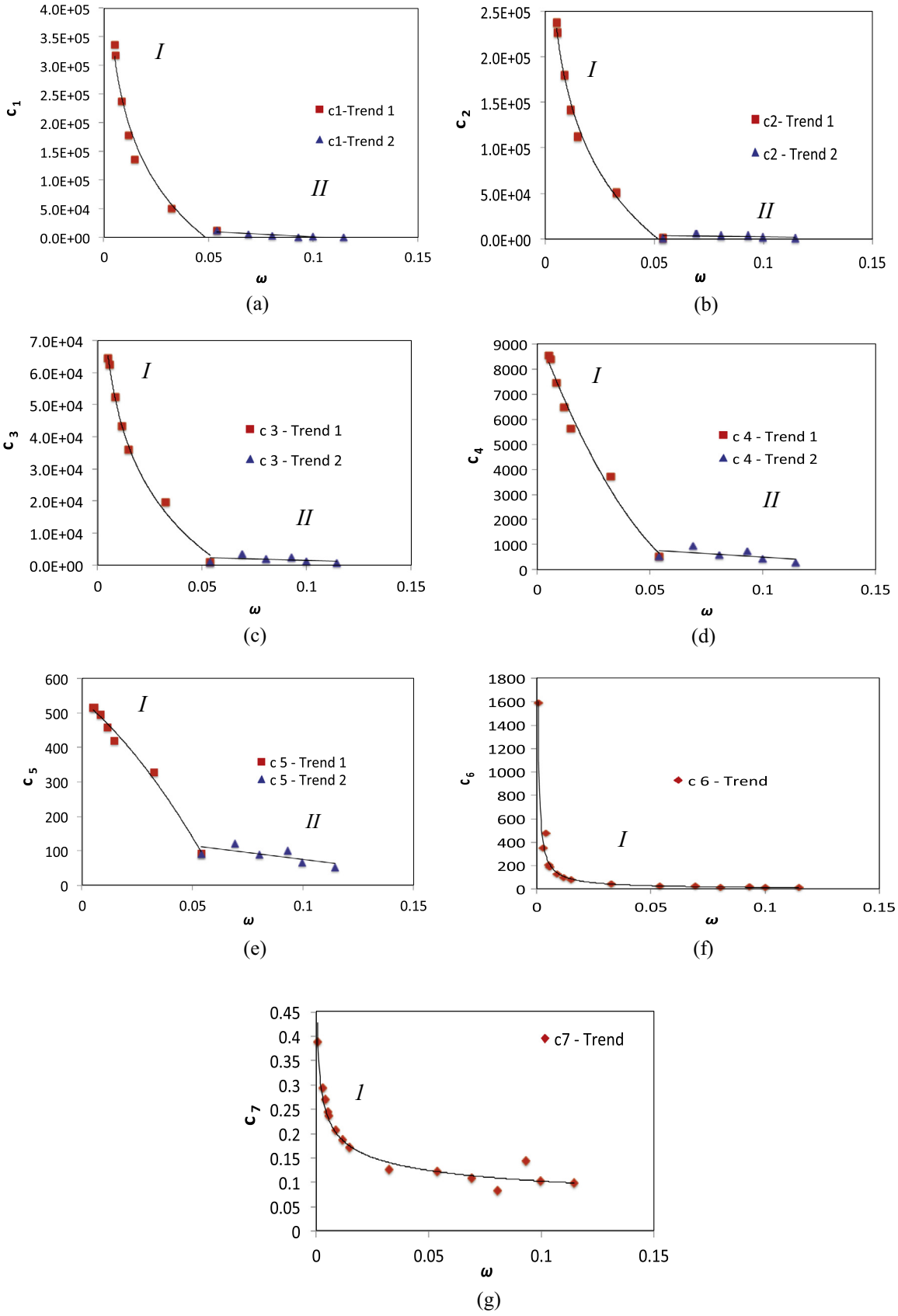

Fig. 4. Variation of coefficients (c1–c7) in Eq. (3) against the ratio of vapour to liquid density (ω) for P < 125 bar: (a) I: $c_1 = -1E{+}05\ln(\omega) - 427{,}619$; II: $c_1 = -185m854\omega + 19{,}121$ (b) I: $c_2 = -1E{+}05\ln(\omega) - 298{,}627$; II: $c_2 = -29m199\omega + 5219.3$ (c) I : $c_3 = -26553\ln(\omega) - 74{,}405$; II: $c_3 = -18{,}088\omega + 3324$ (d) I: $c_4 = -1E{+}06\omega^2 - 237{,}169\ \omega + 9447.6$; II: $c_4 = -5676.6\omega + 1071.4$ (e) I: $c_5 = -51436\omega^2 - 5385.3\ \omega + 538.57$; II: $c_5 = -800.03\ \omega + 155.54$ (f) I: $c_6 = 1.9005\ \omega^{-0.911}$ (g) I: $c_7 = 0.054\ \omega^{-0.28}$.

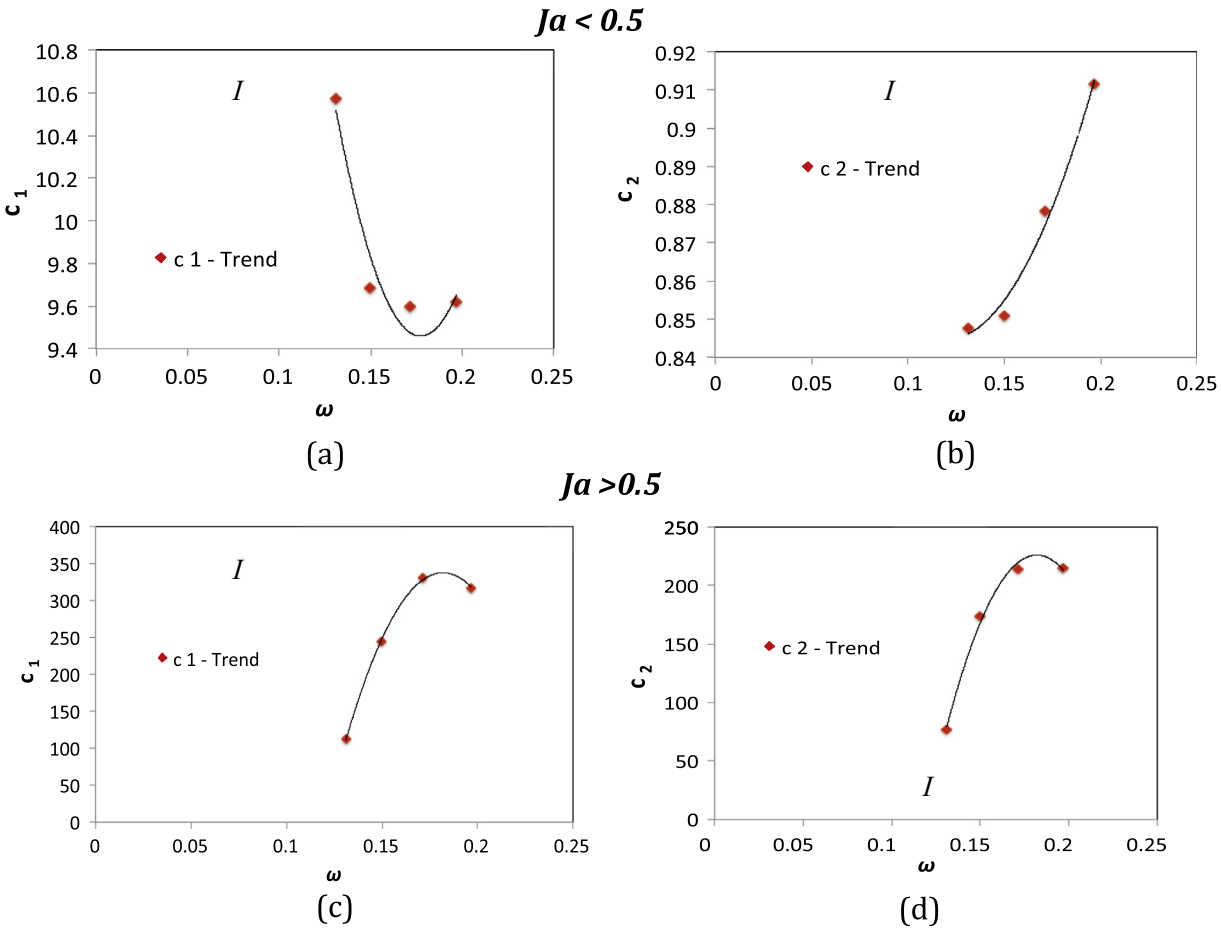

Fig. 5. Variation of coefficients *c1* and *c2* in Eq. (4) and (5) as a function of density ratio (ω) for $P > 125$ bar. (a) I: $c_1 = 497.76\omega^2 - 176.37\omega + 25.083$. (b) I: $c_1 = 11.613\omega^2 - 2.7979\omega + 1.013$. (c) I: $c_1 = -87856\omega^2 + 31948\omega - 2566.8$. (d) I: $c_1 = -56808\omega^2 + 20671\omega - 1654.3$.

Table 1
Summary table of coefficients in the β_{IP} expressions Eq. (3)-(5)

For $\omega \leq 0.115$ (1 bar $\leq P \leq$ 125 bar) $\beta_{IP} = -c_1Ja^6 + c_2Ja^5 - c_3Ja^4 + c_4Ja^3 - c_5Ja^2 + c_6Ja + c_7$		
	$\omega \leq 0.054$	$0.054 < \omega \leq 0.115$
C_1	$-1e^5 ln(\omega) - 427{,}619$	$-185854\omega + 19{,}121$
C_2	$-1e^5 ln(\omega) - 298{,}627$	$-29199\omega + 5219.3$
C_3	$-26553 ln(\omega) - 74{,}405$	$-18088\omega + 3324$
C_4	$1e^6\omega^2 - 237169\omega + 9447.6$	$-5676.6\omega + 1071.4$
C_5	$-51436\omega^2 - 5385.3\omega + 538.57$	$-800.03\omega + 155.54$
C_6	$1.9005\ \omega^{-0.911}$	
C_7	$0.054\ \omega^{-0.28}$	
For $0.115 < \omega$ (125 bar $< P$)		
	$Ja \leq 0.5$	$Ja > 0.5$
	$\beta_{IP} = c_1 Ja^{c_2}$	$\beta_{IP} = c_1 \ln(Ja) + c_2$
C_1	$497.74\omega^2 - 176.37\omega + 25.083$	$-87856\omega^2 + 31{,}948\ \omega - 2566.8$
C_2	$11.613\omega^2 - 2.7979\omega + 1.0133$	$-56808\omega^2 + 20671\omega - 1654.3$

Where $\omega = \frac{\rho_g}{\rho_l}$, $Ja = \frac{c_l T_{sup}}{h_{lg}}$.

layer, we have assumed that the temperature near the microlayer will not be superheated. We believe the microlayer will induce a distortion in the thermal boundary layer as indicated in our Fig.6.

It is to be noted that the terminology of 'thermal layer' that is used in this paper refers to the 'effective'/'cumulative' thermal

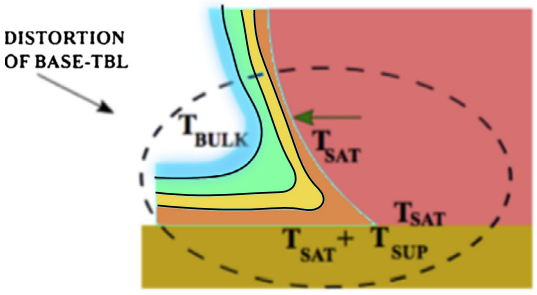

Fig. 6. Distorted base thermal layer near the 'wall – bubble' contact line.

layer (TL) that surrounds the bubble interface. When a bubble is suspended in an infinite pool of superheated liquid, a thermal layer is present adjacent to the bubble interface. The temperature of this TL varies between the saturation temperature of the interface and the superheated temperature of the liquid medium. Similarly, for a bubble that is growing at the wall, a large portion of the bubble interface will have an 'effective' thermal layer in which the temperature will vary between the saturation temperature of the interface and the temperature of the liquid medium. However, near the wall, this 'cumulative' thermal layer temperature will also be influenced by the superheated wall temperature.

Depending on the operating conditions of the system and the surface characteristics, the local/micro complexities of contact line movement might vary. There could be a dryspot formation

and/or a superheated liquid layer present, and these might contribute to the heat transfer during different phases of the bubble ebullition cycle. But, on the 'cumulative' level, when averaged spatially and temporally, for the near-wall region, over the entire bubble ebullition cycle, the temperature difference would be largely between the saturation temperature of the interface, the wall superheat temperature and the bulk fluid temperature. Since the proposed bubble growth model has been developed for application in the averaged two-fluid model framework and for component scale systems, an effective representation of the thermal layer is believed to be sufficient to capture the bubble growth phenomenon. An added advantage would be that a less complex formulation enables better convergence.

Since, the wall effect multiplier attempts to account for the 'effective' thermal layer thickness and not the local/micro-scale contact line related temperature differences, the term of Ja_{sat} is believed to suitably capture the thermal contribution to the thickness of the TL.

- ψ_1 *factor(fluid property component)*: The Ja_{sat} term discussed above, accounts for the thermal component of the wall effect multiplier. In addition to this, fluid properties also contribute to the multiplier. Hence, the present model uses the ψ_1 factor to capture this fluid property contribution. When the fluid property changes, there is a change in the shape of the bubble, which in turn is influenced by the phenomena contributing to it. In this context, it is worth recapitulating the experimental observation of Akiyama et al. [1]. They have observed that, the shape of the bubble changes with pressure, wherein the bubble is flatter at low pressures, but the sphericity increased with increase in system pressure. They have also observed that, the bubbles grow at a faster rate at low pressures than at higher pressures. The increase in growth rate at low pressures was attributed to the presence of microlayer near the bubble base [1]. From all the aforementioned observations of Akiyama et al. [1], it is apparent that the flatness of the bubble, the presence of the microlayer and the increased growth rate are closely interlinked. Additionally, it can also be surmised that the change in the shape of the bubble essentially influences the shape of the thermal layer surrounding the bubble and this change in thermal layer shape is what causes the change in the growth rate. It is estimated that, the increased growth rate observed by Akiyama et al. [1] is because the TL becomes thinner due to the flatness of the bubble and due to the presence of the microlayer. On the whole it can be concluded that, the shape of the bubble significantly influences the ψ_1 factor and this influence is translated into an effect on the growth rate through a change in the size of the TL. Hence, some of the observed growth rate trends from the literature are incorporated in modeling ψ_1 as it is adequately linked to the likely change in the TL and bubble shape.

  Akiyama et al. [1] predicts a linear decrease in his bubble growth constant (similar to β_{IP}) for water till a pressure of 10 atm. However, from the literature it is unclear if this linear trend continues at higher pressures. A hypothesis of the growth rate trend may be made from the growth constant (β_{IP}) plotted in Fig. 2, which depicts a non-linear decrement with pressure. Additionally, the trend of the leading constant c_1 of β_{IP} approximates a trend similar to the hyperbolic curve. This major trend is adopted in modeling ψ_1 as $\sim \frac{1}{\sqrt{\omega}}$. The hypothesis of non-linear decrease of growth rate can be further corroborated from the experimental data of Sakashita [41] for pressures ranging from 19 to 45 bar.
- Since the trend is established, suitable coefficients which fit the trend need to be obtained. This is achieved as follows. The temperature of the bulk fluid governs the TL shape, and in turn influences the temperature gradient of the fluid present within the TL region. However, T_{bulk} could be saturated, superheated or subcooled and the trend of the variation in temperature gradient with pressure for each of these cases could be different. Hence, the model incorporates experimental data [44,17], where fluid bulk is either superheated or saturated. For the various values of ψ_1 determined across the pressure range, a fitting curve is generated with a trend of $\sim \frac{1}{\sqrt{\omega}}$. The ψ_1 values predicted for saturated and superheated cases were more or less close to each other. However, average values are chosen when they are not close to each other. The fitting curve also appeared to support the hypothesis of the $\sim \frac{1}{\sqrt{\omega}}$ trend, as depicted in Fig. 7.

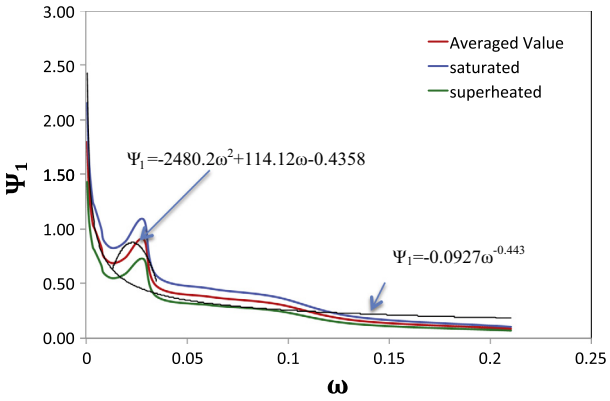

Fig. 7. Variation of fluid property component (Ψ_1) of the wall effect multiplier against density ratio (ω).

- From the trend of ψ_1 values observed in Fig. 7, a deviation from the $\frac{1}{\sqrt{\omega}}$ trend can be noticed in the pressure range of 20–40 bar. In this pressure range, the trend has a kink with an increase and a decrease of ψ_1 as shown in Fig. 7. It should be pointed out that, the wall effect multiplier must account for the contact angle effect which is perhaps responsible for the increase and decrease in growth rate in this pressure range. Bernadine et al. [4] in their experimental study analysed the variation of bubble contact angle with increasing temperature. Their study shows that, the cosine of the contact angle reduces as a function of temperature ($\sim T^{0.469}$) (Fig. 8). Additionally, it is observed from Sakashita's [41] experiments that, the bubbles become increasingly spherical in the pressure range between 20 and 40 bar, indicating lower bubble contact angles. At very low contact angles, it can be surmised that, the bubble interface is very close to the wall and facilitates an increased heat transfer and hence higher growth rate. This is supported by the experimental observations of Mukherjee and Kandlikar [32], wherein the lowering of contact angle resulted in an increase in heat transfer. All these observations substantiate the sudden rise in growth rate as predicted by the ψ_1 values, thus accounting for the contact angle effect. However, with further increase in pressure, a further decrease in contact angle was noticed, as the bubble is more spherical at higher pressures. Hence, the bubble remains tighter and smaller. Therefore, the growth rate begins to drop once again. This explains sudden increase and then a decrease in growth rate trend in this pressure range. This aspect is modeled through the expressions presented in Table 2, which follows the trend depicted in Fig. 7.
- f_1 factor (fluid component) : To be able to account for both pool and flow boiling conditions, the f_1 factor was introduced. For pool boiling conditions, this factor is set to 1. However, under the influence of flow, near wall TL is modified. This modification is introduced in the model through f_1. This is accounted in a

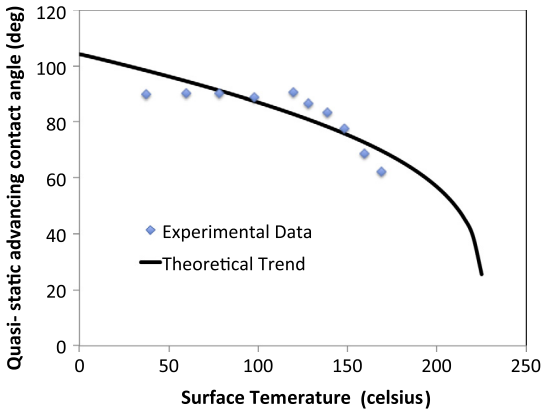

Fig. 8. Contact angle (θ) variation with surface temperature. Note in particular, a sudden decrease of Quasi-static contact angle at high surface temperature of 120–160 °C (redrawn from Bernadine et al. [4]).

passive way through the Prandtl number (*Pr*) and in an active way through the Base Thermal Layer Flow Distortion Factor (BD i.e. $\frac{1}{e^{\tau}}\left(\frac{\delta u}{\eta}\right)^{n_1}$). In the context of bubble growth, when convection is absent, heat transfer is predominantly through conduction. Here, the relative strength of convection to conduction heat transfer is exemplified through the Prandtl number. However, it is a passive term, which is in terms of the fluid properties alone and does not account for the fluid velocity. Hence, an active term based on fluid velocity and wall superheat is formulated as $\left(\frac{\delta u}{\eta}\right)^{n_1}$. This exemplifies the convective component of the thermal transport to the thermal diffusivity effects. Although δ refers to the mixed convection thermal boundary layer, for the ease of computation, it is assumed that this value is close to the natural convection thermal boundary layer thickness δ ($\delta = 7.14\left(\frac{\nu_l \eta_l}{g\beta_{exp}\Delta T}\right)^{1/3}$, [31]). This active term qualitatively represents the influence of flow on growth rate. Hence, the term $\frac{1}{e^{\tau}}\left(\frac{\delta u}{\eta}\right)^{n_1}$ is considered to represent the distortion of the base TL, due to flow, as shown in Fig. 9(c). This distortion would in turn reflect on the growth rate of the bubble. The multiplier $\frac{1}{e^{\tau}}$ is added to the formulation to account for the strength of subcooling effect, where $\tau = \frac{\Delta T_{sub}}{\Delta T_{sup}+\Delta T_{sub}}$ (further discussed in Section 3.2.3). When the liquid is close to saturation, there will be no subcooling effect and hence this term should become 1. At the same time, when subcooling is very high (~80 K) then, it causes quick condensation and hence causes a decrease in growth rate. Therefore in a modeling sense, variation from high to low 'τ', should vary the multiplier from a very low value to a value tending to 1, which is captured through $\frac{1}{e^{\tau}}$ multiplier . It is to be noted here that the 'distortion' of the thermal layer is expressed relative to a pool boiling case (see Fig. 9(b) and (c)), for the same operating conditions. Due to the combined effect of the flow and subcooling, the percolation effect of the cold bulk fluid towards the wall is high and is felt closer to the bubble base. The modeled f_1 factor is summarized in Eq. (6) for both pool boiling as well as flow boiling conditions.

$$f_1 = \begin{cases} 1 & \text{for pool boiling} \\ \left(\frac{1}{e^{\tau}}\right)\left(\frac{\delta u}{\eta}\right)^{n_1} Pr^{\frac{1}{3}} & \text{for flow boiling} \end{cases} \quad (6)$$

3.2.3. Bulk effect multiplier (ψ_{bulk})

The wall effect multiplier characterized the distortion of the TL in the immediate vicinity of the wall-bubble contact line. However, it is also observed that the TL surrounding the rest of the bubble also undergoes distortion, particularly when the bulk fluid is subcooled.

Prior to bubble nucleation at the wall, a thermal boundary layer (TBL/TL) already exists at the wall. The temperature inside this TL varies from the wall superheated temperature to the bulk fluid temperature. This thermal boundary layer is known as the "Wall-TL component". When the bubble first nucleates, the liquid-vapour interface that is formed will be at the saturation temperature. It is to be noted that in the present work, this liquid-vapour interface is divided into two regions: (i) The bubble interface near the wall (base) and (ii) the interface at the top (apex) of the bubble. The latter is called the 'bubble apex interface'. The TBL, which the bubble apex interface is initially exposed to, has temperatures varying from superheated temperature to the bulk fluid. However, the interface itself is at the saturation temperature. Hence, at the apex interface of the bubble, the thermal boundary layer readjusts during the bubble ebullition cycle from $((\Delta T_{sup} + T_{sat}) - T_{bulk})$ to $(T_{sat} - T_{bulk})$. The averaged thickness of TBL during the period of the entire bubble ebullition cycle will lie between these thicknesses and is termed as the "effective thermal layer at bubble apex". This distortion is really prominent near the apex of the bubble, which is characterized through the bulk effect multiplier as follows:

$$\chi_1\tau - \left[\left(\frac{(2\beta_{IP}\sqrt{\eta t})(\beta_{IP}\sqrt{\tau})\omega}{\delta}\right)\tau f_2\right] \quad (7)$$

It can be noticed that bulk effect factor comprises of two terms. While the first term ($\chi_1\tau$) is representative of the thickness of the thermal boundary layer formed at the wall due to temperature difference between the wall and the bulk fluid, the second term is representative of the bubble apex interface moving upwards, as it grows into the subcooled fluid layers as shown in Fig. 10. The difference between the two gives the effective thermal layer for the apex of the bubble. The formulation of these terms is discussed separately as follows.

- *Wall-TL component* ($\chi_1\tau$): The temperature difference between the wall and the subcooled liquid will dictate the thickness of the thermal boundary layer (δ). In order to represent this thickness in terms of the strength of subcooling τ, the multiplier χ_1 is introduced. χ_1 essentially captures the reduction in size of τ with pressure. To be able to estimate the variation of χ_1,the following assumption is made. The driving force represented by τ is assumed to be synonymous to $c_1 Ja^6$, which represents the bubble growth factor . It should be pointed out that, while τ drives the wall thermal boundary layer (TBL) development, the infinite medium bubble growth is driven by the β_{IP} factor. Hence a formulation similar to that of the c_1 was adopted and on fitting with a few subcooled bulk experimental cases (see Wu and Dhir [54] for data from [38]) the expression $\chi_1 = -1.211\ln(\tau) - 0.048$ was obtained.

Table 2
Variation of fluid property component (Ψ_1) of the wall effect multiplier as a function of density ratio (ω).

Ψ_1	$\omega \leq 0.013$ $0.0927\omega^{-0.443}$	$0.013 < \omega < 0.035$ $(-2480.20\omega^2 + 114.12\omega - 0.4358)$	$\omega \geq 0.035$ $0.0927\omega^{-0.443}$	$Ja_{sat} = \frac{c_l T_{sat}}{h_{fg}}$

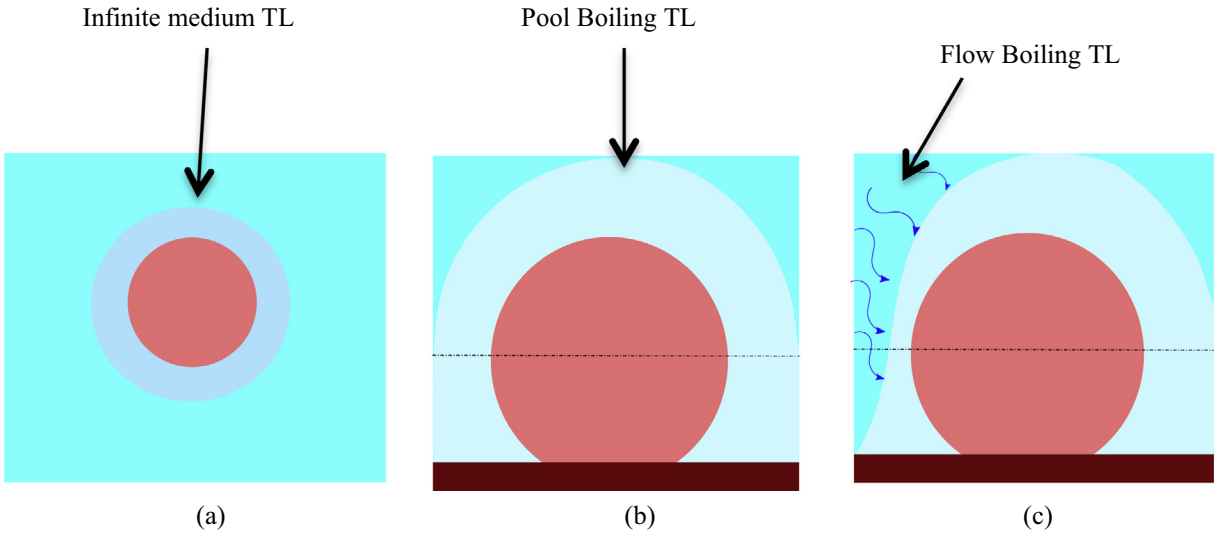

Fig. 9. Bubble TL – (a) undistorted bubble in an infinite superheated medium (b) base thermal layer distortion under pool boiling conditions (c) Both base and apex thermal layer distortion under flow boiling condition.

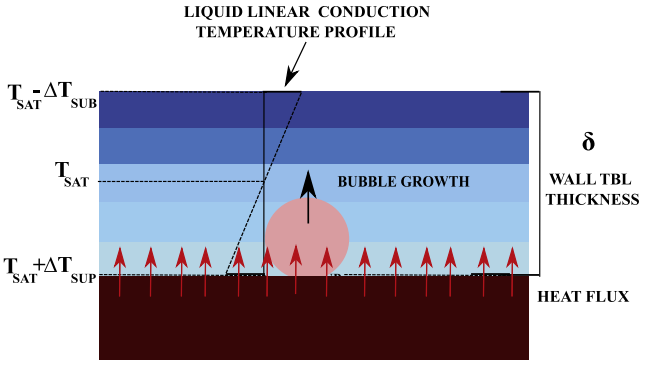

Fig. 10. Schematic for bubble growth against 'strength of subcooling' factor τ.

- *Bubble apex interface movement component:* When a bubble starts to grow, there is a TL surrounding the bubble interface. This TL at the apex transitions from saturation temperature at the bubble interface to the bulk fluid temperature. The effective TL is a resultant of the interaction between the wall TBL and the bubble TL. Thus, the upward movement of the bubble apex interface is accounted by the term: $\left[\left(\frac{(2\beta_{IP}\sqrt{\eta t})(\beta_{IP}\sqrt{\tau})\omega}{\delta}\right)\tau f_2\right]$. In this expression, $(2\beta_{IP}\sqrt{\eta t})(\beta_{IP}\sqrt{\tau})\omega$ qualitatively represents the radius of the bubble as it grows. This term is a combination of the infinite bubble growth model, with corresponding modifiers for the wall and subcooling effect $(\beta_{IP}\sqrt{\tau})$ as well as the pressure effect (ω). Here, the formulation of $(\beta_{IP}\sqrt{\tau})$ is proposed to be similar to $\beta_{IP}\sqrt{\eta}$, where the infinite bubble growth component is driven by β_{IP} and the diffusivity of the fluid $(\sqrt{\eta})$ .Similarly at the interface of the apex, the bubble growth is likely to be governed by the strength of the subcooling as well as the wall superheat. Hence, the term accounts for both the effects. Hence, the ratio $\left(\frac{(2\beta_{IP}\sqrt{\eta t})(\beta_{IP}\sqrt{\tau})\omega}{\delta}\right)$ is indicative of the portion of the wall TBL that the growing bubble will occupy. This fraction of the distance is then expressed in terms of the subcooling strength τ.

For pool boiling conditions, the effective TL constantly evolves with time and hence, the fluid adjacent to the interface is constantly in motion or being churned. Additionally, growth rate of bubbles will be affected by the wake of the preceding bubbles, which is particularly prominent at the apex of the bubble. This effect is included in the bulk effect parameter as ω^{b_1} (Table 3) and is termed as wake effect multiplier. Since the fluid circulation changes with pressure, the wake effect multiplier is formulated using ω. To this end, experimental test case in subcooled, saturated and superheated bulk category are chosen (Fig. 11) and fitting parameters are identified. An overall variation in ω^{b_1} trend for all the three cases is presented in Fig. 11 as well as Table 3.

It should be pointed out that, the wake effect is accounted only for pool boiling and not for flow boiling. In reality, wake is observed, when a bubble departs vertically from a horizontal wall under pool boiling conditions. However, bubble sliding is likely under flow boiling as well as vertical pool boiling conditions. In the present model, the bubble is assumed to be attached to the nucleation site for the entire period of its growth and detaches normal to the wall under all the operating conditions. However, for the vertical pool boiling and flow boiling cases, the bubbles will not

Table 3
Pool boiling: wake effect multiplier ω^{b_1}.

ω^{b_1}	
b_1	Superheated bulk
$\omega < 0.0130$	$-3.4382\omega + 0.0953$
$0.0130 \Leftarrow \omega < 0.0280$	$-2657.9\,\omega^2 + 119.97\,\omega - 1.059$
$0.0280 \Leftarrow \omega < 0.0350$	$-31.5\,\omega + 1.1112$
$0.0350 \Leftarrow \omega < 0.0940$	$-16.296\,\omega^2 + 2.6928\,\omega - 0.0642$
$0.0940 \Leftarrow \omega$	$-13.393\,\omega^2 + 8.8385\,\omega - 0.6659$
b_1	Saturated bulk
$\omega < 0.0130$	$-11.335\omega + 0.1086$
$0.0130 \Leftarrow \omega < 0.0210$	$-1058.7\omega^2 + 42.715\,\omega - 0.4302$
$0.0210 \Leftarrow \omega < 0.0350$	$-1594.9\,\omega^2 + 69.86\,\omega - 0.7636$
$0.0350 \Leftarrow \omega < 0.0940$	$-16.296\,\omega^2 + 2.6928\,\omega - 0.3447$
$0.0940 \Leftarrow \omega$	$-13.393\,\omega^2 + 8.8385\,\omega - 0.9464$
b_1	Subcooled bulk
$\omega < 0.0130$	$-11.835\omega + 0.0488$
$0.0130 \Leftarrow \omega < 0.0210$	$-952.36\omega^2 + 39.609\,\omega - 0.4687$
$0.0210 \Leftarrow \omega < 0.0350$	$-1594.9\,\omega^2 + 69.86\,\omega - 0.8247$
$0.0350 \Leftarrow \omega < 0.0940$	$-16.334\,\omega^2 + 2.6987\,\omega - 0.406$
$0.0940 \Leftarrow \omega$	$-13.393\,\omega^2 + 8.8385\,\omega - 1.0075$

Table 4
Expressions for the variation of Ψ_{bulk} against strength of subcooling τ.

	$\tau \to 0$	$0 < \tau < 1$	$\tau \to 1$
Pool boiling Ψ_{bulk}	$(1 - 2\beta^2\omega\frac{\sqrt{\eta t}}{\delta}\tau^{1.5}f_2)\omega^{b_1}$	$\left(\chi_1\tau - \left(\left(\frac{2\beta\sqrt{\eta t}}{\delta}\right)\beta\omega\tau^{1.5}f_2\right)\right)\omega^{b_1}$	0
Flow boiling Ψ_{bulk}	$\left(1 - 2\beta^2\omega\frac{\sqrt{\eta t}}{\delta}\tau^{1.5}f_2\right)$	$\left(\chi_1\tau - \left(\left(\frac{2\beta\sqrt{\eta t}}{\delta}\right)\beta\omega\tau^{1.5}f_2\right)\right)$	0

$\chi_1 = -1.2110\ln(\tau) - 0.0480$, $\omega = \frac{\rho_g}{\rho_l}$, $\tau = \frac{\Delta T_{sub}}{\Delta T_{sup}+\Delta T_{sub}}$.

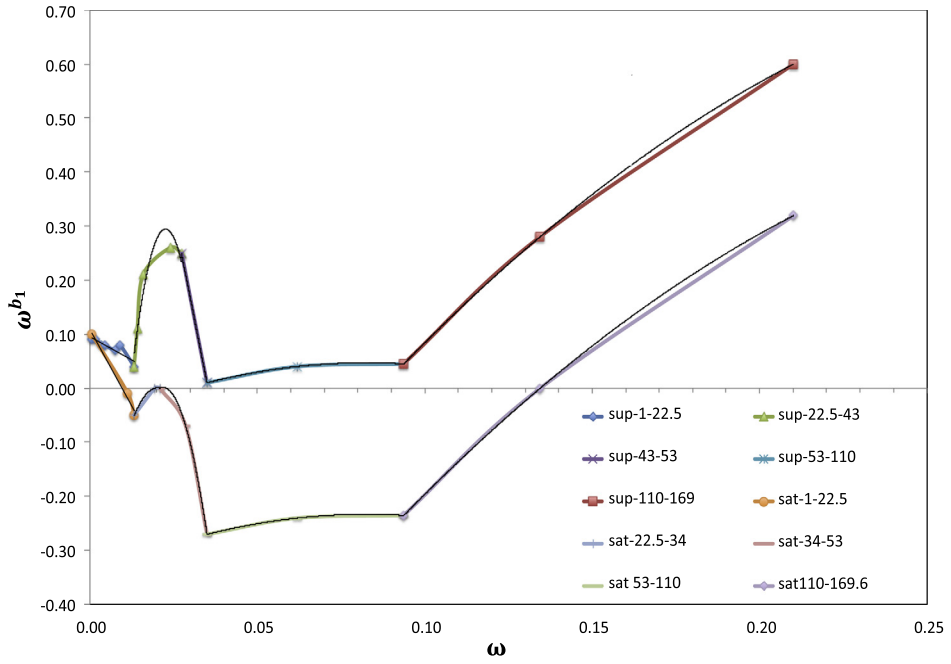

(a)

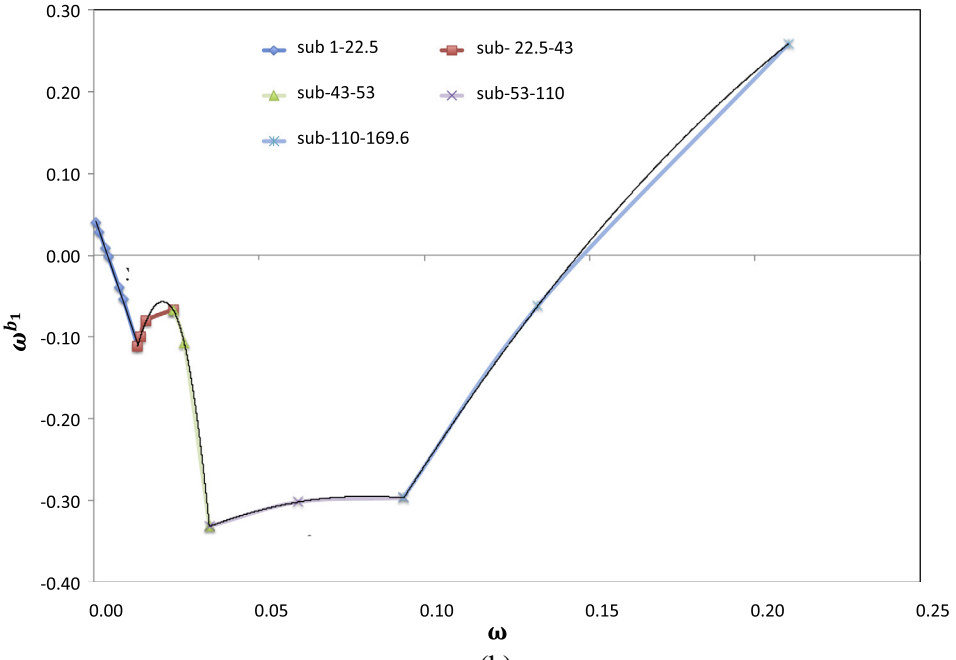

(b)

Fig. 11. Curves generated for ω^{b_1} for (a) superheated, saturated (b) subcooled fluid conditions.

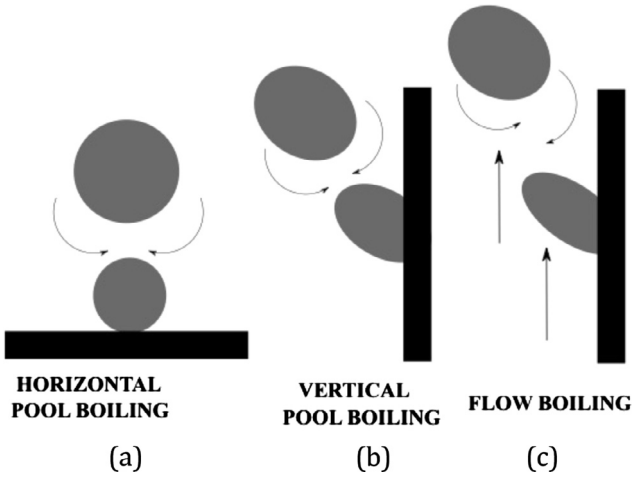

Fig. 12. Depiction of the extent of exposure of the bubble to the wake effect in (a) horizontal pool boiling (b) vertical pool boiling (c) flow boiling.

detach perpendicular to the wall, and hence, the wake will not be able to directly influence the subsequent bubble. Moreover, the wake effect convecting towards upstream will result in damping effect. Since the wake effect is deflected and confined (see Fig.12), a large part of the bubble interface of the subsequent bubble will not see any wake effect. Hence, in our formulation, the wake effect for flow boiling is not accounted.

- f_2 factor: For the case of flow boiling, the bulk fluid motion overrides the circulation and the wake effect multiplier. As the bubble grows, maximum bulk effect due to the flow is felt at the upper interface TL, in particular when the fluid is subcooled. Hence, the modifier f_2 factor is formulated in terms of the strength of subcooling as follows:

$$f_2 = \left[\tau^{2.5}\left(\frac{\delta u}{\eta}\right)^{n_2} Pr^{0.33}\omega(1716.60e^{-0.0270\omega})\right] \tag{8}$$

The term $\tau^{2.5}\left(\frac{\delta u}{\eta}\right)^{n_2}$ refers to Apex Thermal Layer Flow Distortion Factor (AD) and is modeled similar to the Base Distortion (BD) effects. Hence, AD indicates apex distortion effects relative to an equivalent pool boiling thermal layer. The apex growth for pool boiling already accounts for the effects of wall superheat, subcooling and pressure effect as $\beta_{IP}\sqrt{\tau\omega}$. However, in the presence of flow, the subcooling effect mainly contributes to the distortion of the TL. To account for this increased effect of subcooling, $\tau^{2.5}$ is used as a multiplier for the AD term. Additionally, the wall effect and pressure effect are also modified under flow boiling conditions. Hence $\beta_{IP}\sqrt{\tau\omega}$ component is modified by fitting with experiments [7,48,28] using the multiplier $[\omega(1716.6e^{-0.027\omega})]$. Hence, the flow effect multiplier has the following form

$$f_2 = \begin{cases} 1 & \textit{Pool Boiling} \\ 1716.60\omega e^{-0.0270\omega}\tau^{2.5}\left(\frac{\delta u}{\eta}\right)^{n_2} Pr^{\frac{1}{3}} & \textit{Flow Boiling} \end{cases} \tag{9}$$

3.3. Summary of the formulation

The present model accounts for three main changes to the infinite medium bubble growth: (i) Flow effect, (ii) subcooling effect and (iii) variation with pressure. The effect of each of these parameters is modeled for both the near-wall bubble interface, as well as the bubble apex interface (see Table 5).

3.4. Notes on modeling specifics

i. The infinite bubble growth component of the present model assumes that the bubble is surrounded by liquid, which is at a uniform superheat (which is essentially the wall temperature in the present case). However, in reality, for a bubble growing at the wall, only a part of its interface will be exposed to this superheat temperature (i.e. mainly the bubble interface that is directly in contact with the heater surface). The rest of the interface would be exposed to fluid at a temperature different from the wall superheat. This difference will result in a deviation of the actual growth rate from the idealized growth prediction in an infinite medium. The extent of this 'deviation' will depend on the pressure, subcooling and flow conditions of the system. Hence, wall effect multiplier has been introduced to account for these effects using 3 parameters viz., J_{sat}, ψ_1 *and* f_1. They account for the deviation due to liquid temperature, the pressure, the flow parameters and fluid velocity respectively.
ii. Since the present model has been developed to predict bubble growth in the pressure range of 1–180 bar, the emphasis is on the heat diffusion controlled growth phase of the bubble and not the inertia controlled growth phase. It has been found in literature [43] that the inertia controlled growth phase occupies a very small portion of the bubble growth. Moreover, this proportion decreases as pressure increases. Consequently, the present model does not account for the inertia controlled growth phase of the bubble.
iii. In most flow boiling and vertical pool boiling cases, the bubbles slide and depart. However, the model proposed in this paper assumes that the bubble remains attached to the nucleation site for the entire period of its growth and does not slide. The sliding based growth was not modeled as most experimental data for sliding based growth is available only at or near atmospheric pressures and not for higher pressures. Also, it is the general understanding that the bubbles are more dynamic (e.g. sliding) at or near atmospheric pressures and with increasing pressure they tend to grow slower and remain attached to the nucleation site.

4. Bubble growth prediction

The detailed formulation discussed in Section 3 is now subjected to bubble growth rate predictions for the entire pressure range of 1–180 bar. It should be pointed out that, the experimental literature on high pressure, is really sparse. Therefore, the present model is promising as it accounts for the phenomenological features of bubble growth to cover the entire pressure range.

4.1. Pool boiling conditions

From pool boiling experiments, in the literature, the factors contributing to bubble growth were found to be - operating pressure, temperature of the fluid (superheated, saturated and subcooled), wall superheat, orientation of the test section etc. By taking these factors into account, various pool boiling conditions are compiled in Table 6. The change in the radius of the bubble with time as predicted by the present phenomenological model, is compared against the experiments. In studies where only the radius of the bubble at a fixed time level was available, the current model's predicted radius at that specified time was compared.

Table 5
Summary of physics accounted in the mathematical model development.

Type of boiling	Physics accounted for	Parameters for wall effect ($Ja_{sat}\psi_1$)	Parameters for bulk effect $\psi_{bulk} = \chi_1\tau - \left(\frac{2\beta_{IP}\sqrt{\eta t}}{\delta}\beta_{IP}\omega\tau^{1.5}\right)$	
			($\chi_1\tau$)	$\left[\left(\frac{(2\beta_{IP}\sqrt{\eta t})(\beta_{IP}\sqrt{\tau})\omega}{\delta}\right)\tau\right]$
Pool (no flow)	Effect of pressure variation	ψ_1 (see Table 2)	χ_1 (see Table 4)	$\left(\frac{(2\beta_{IP}\sqrt{\eta t})(\beta_{IP}\sqrt{\tau})\omega}{\delta}\right)$ Comprises of 2 components: • Infinite medium growth component: $2\beta_{IP}\sqrt{\eta t}$ where β_{IP} has inbuilt pressure effect • $\beta_{IP}\sqrt{\tau}\,\omega$: Here, $(\beta_{IP}\sqrt{\tau})$ is wall and subcooling effect; ω is pressure effect (see Table 4)
	Effect of subcooling	No subcooling effect at wall	$\chi_1 = fn\,(\tau)$ includes subcooling effect	
	Wake effect of previous bubbles	No wake effect at wall	ω^{b_1} (see Table 3)	
Flow	Effect of pressure variation	ψ_1 (see Table 2)	χ_1 (see Table 4)	• Same as pool boiling except f2 $f_2 = \tau^{2.5}\omega(1716.60e^{-0.0270\omega}) * \left(\frac{\delta u}{\eta}\right)^{n_2} Pr^{0.33}$ • $\tau^{2.5}$: flow + subcooling effect • $\omega(1716.6e^{-0.027\omega})$: wall + pressure effect on growth component
	Effect of subcooling is coupled with flow	$f_1 = \left(\left(\frac{1}{e^{\tau}}\right)\left(\frac{\delta u}{\eta}\right)^{n_1} Pr^{0.33}\right)$		
	Wake effect of previous bubbles	No wake effect	No wake effect at the apex as flow effect is dominant.	

Table 6
Test database for pool boiling bubble growth experiments.

Experiment	Pressure (bar)	Wall superheat (K)	Liquid temperature (K)	Subcooling (K)	Orientation
Dergarabedian [13]	1.0	3.1	Superheated	–	Vertical beaker
Hooper and Abdelmessih (see Ref. [21])	1.0	13.0	Saturated	–	Horizontal
Ramanujapu [38] (from Wu and Dhir [54])	1.0	6.5 7.0	Subcooled	4.0 1.5	Horizontal
Slooten [44]	2.8 5.9 7.5 12.7 15.2 22.3 23.7 38.3 43.0	1.3 2.2 2.4 2.8 2.9 3.2 3.5 3.7 5.0	Saturated	–	Horizontal
Sakashita [41]	22.3 31.7 44.7	2.7 2.3 1.8	Saturated	–	Horizontal
Sakashita [41]	19.1 34.0	4.7 4.0	Saturated	–	Vertical
Griffith [17]	26.4 53.0 83.0 110.5 136.9 169.6	34.8 30.5 21.4 19.6 13.8 6.2	Superheated	–	Horizontal

4.1.1. Bubble growth: under atmospheric conditions

Dergarabedian's [13] has experimentally obtained the bubble growth rate of a bubble rising in a column of water, for various superheats, under atmospheric conditions. These test conditions are comparable to the ideal scenario of bubble growth in an infinite superheated medium. Fig. 13(a) presents the growth rate predictions of the current model against these experiments for a uniformly superheated temperature of 3.1°c. Although there is a marginal over prediction, overall a good comparison can be noticed. Hooper and Abdelmessih (see Ref. [21]) conducted experiments on bubbles growing at the wall under saturated boiling and atmospheric conditions. Corresponding predictions are shown in Fig. 13(b). Wu and Dhir [54] conducted simulations and compared them against experiments [38] of a bubble growing at the wall in a subcooled bulk. Under these conditions, the bubble is initially submerged in a portion of the TBL that is predominantly superheated. However, as the bubble grows, the apex of the bubble will eventually come in contact with the subcooled liquid and hence, undergoes condensation at that interface. This causes a decrease in the growth rate of the bubble. Hence, the growth curve plateaus as shown in Fig. 13(c). Thus, the present model is able to capture the bubble growth even in subcooled pool boiling conditions at standard atmospheric pressures.

4.1.2. Bubble growth: elevated pressures

Bubble growth studies for pressures higher than atmospheric pressure (2.77–43 bar) was conducted by Slooten [44]. The bubble radius as predicted by the current model (at a specific time level) is

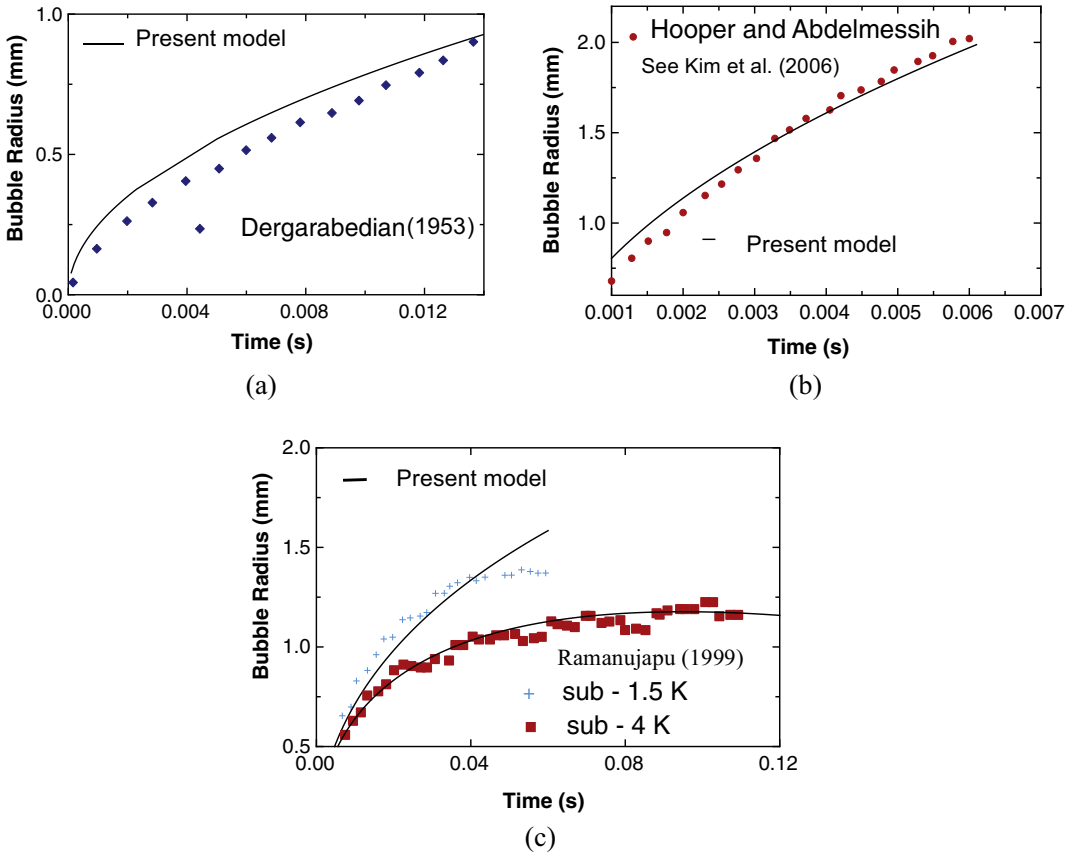

Fig. 13. Comparison of experiment and model predictions for the bubble growth at atmospheric pressure for (a) bubble rising in superheated bulk (b) bubble growing at the wall in saturated bulk (c) bubble growing at the wall in subcooled bulk.

Table 7
Comparison of bubble radius of Slooten's [44] experiment with model prediction.

Pressure (bar)	Experiment R (mm)	Predicted R (mm)	% Deviation
2.8	0.508	0.497	+2.16
5.9	0.573	0.570	+0.52
7.5	0.572	0.562	+1.74
12.7	0.547	0.549	−0.36
15.2	0.519	0.561	−8.10
22.5	0.430	0.395	+8.13
23.7	0.411	0.412	+0.24
38.3	0.406	0.357	+12.10
43.0	0.498	0.524	−5.22

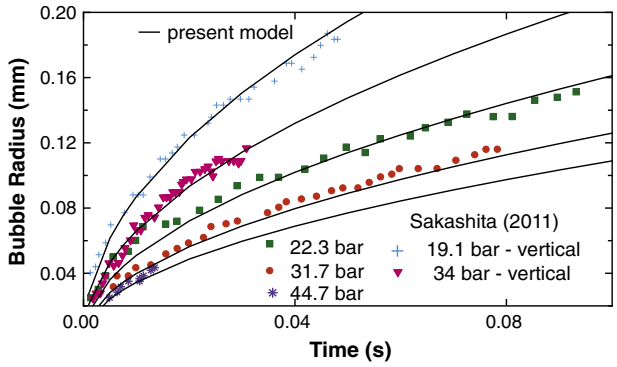

Fig. 14. Comparison of experiment and model predictions for growth at elevated pressure for bubble growing at wall in saturated bulk.

compared with those of the experiments' (Table 7). It can be noticed that, overall, the model is able to predict the bubble radii's for water under superheated conditions at elevated pressures (within 10% with a maximum deviation of 12% at 38 bar).

Sakashita [41] conducted pool boiling experiments at elevated pressures under saturated conditions for both horizontal and vertical test section orientations. The bubble growth predictions from the present model are compared against the experimental study of Sakashita [41] as shown in Fig. 14. The predictions from the present model are particularly promising for vertical pool boiling at higher pressures of 35 bar.

4.1.3. Bubble growth: under high pressures

High pressure pool boiling experiments are almost non-existent in the literature. However, for the sake of completeness of the present study, mathematical model of Griffith [17] is presented for determining the bubble growth rate at the wall for varying pressure conditions. However, these predictions from the present model are compared against Griffith's mathematical model at the point of bubble departure, as presented in Table 8. A reasonable comparison can be noticed. From the present phenomenological model, bubble growth trend was obtained as shown in Fig. 15.

Table 8
Comparison of bubble radius for Griffith [17] mathematical model prediction.

Pressure (bar)	Griffith [17] R (mm)	Predicted R (mm)	% Deviation
53.0	0.033	0.033	0
83.0	0.028	0.028	0
110.5	0.025	0.024	4.00
136.9	0.021	0.021	0
169.6	0.016	0.015	6.25

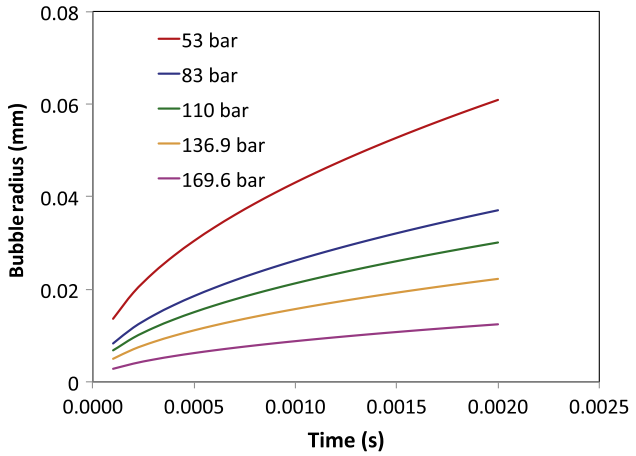

Fig. 15. Bubble size variation with time for different pressures (comparison against Griffith [17] is shown in Table 8, at the point of bubble departure).

4.2. Flow boiling

Under flow boiling, the present wall-bubble growth model is evaluated for several pressures, subcooling and velocities. Since subcooling and fluid velocities are the dominant factors for flow boiling, it is categorized into low and high subcooling followed by low, medium and high velocities. Based on the availability and spread of growth rate data, subcooling of <10 K is considered low subcooling and above it is considered as high subcooling. Similarly, bulk flow velocity (u), u < 1.0 m/s is categorized as low velocity, u = 1–3 m/s as medium velocity and u > 3 m/s as high velocity. Table 9 summarizes the details of the experimental test data employed in the present study.

4.2.1. Flow boiling: low subcooling

Test cases from the experiments of Cao et al. [7] are used to evaluate the model at low subcooling-low velocity conditions. Fig. 16(a) shows that there is good agreement between the experiments and the predictions of the present model.

Further, the model is tested here for marginally higher pressure (1.95 bar), medium velocity (1.15 m/s) and low subcooling (1.95 K) conditions. The predictions are compared against the experimental data of Abdelmessih (see Ref. [28]) as shown in Fig. 16(b). For both low and medium velocities, the low subcooling conditions have shown an initial bubble growth followed by a condensation of the bubble. These features are well predicted through the present phenomenological model.

Table 9
Test database for flow boiling bubble growth.

	Experiment	Pressure (bar)	Wall Superheat (K)	Subcooling (K)	Velocity (m/s)	Test section
Low subcooling–low velocity (LS-LV)	Cao et al. [7]	1.0	9.9 12.4	5.0	0.14 0.44	Vertical-annulus
Low subcooling-medium velocity (LS-MV)	Abdelmessih (see Ref. [28])	1.0	7.7	1.9	1.15	Round tube
Low subcooling-high velocity (LS-HV)	Unal [48]	139.0 139.0 139.0 139.0 158.0 177.0	3.5 3.7 3.9 3.5 4.2 5.2	3.7 4.3 3.7 5.9 4.1 3.0	3.27 3.27 3.27 3.27 3.57 3.75	Round tube
High subcooling–low velocity (HS-LV)	Cao et al. [7]	1.0	3.6	39.3	0.15	Vertical-annulus
	Prodanovic et al. [36]	3.0	13.4	29.4	0.41	Vertical - annulus
High subcooling-medium velocity (HS-MV)	Mayinger and Bucher (see Ref. [28])	2.1	30.0 37.0 38.0	20.0 20.0 40.0	1.00 2.00 1.00	Annulus
High subcooling-high velocity (HS-HV)	Gunther (see Ref. [28])	1.7	16.24 31.23	86.0 86.0	3.05 3.05	Square channel

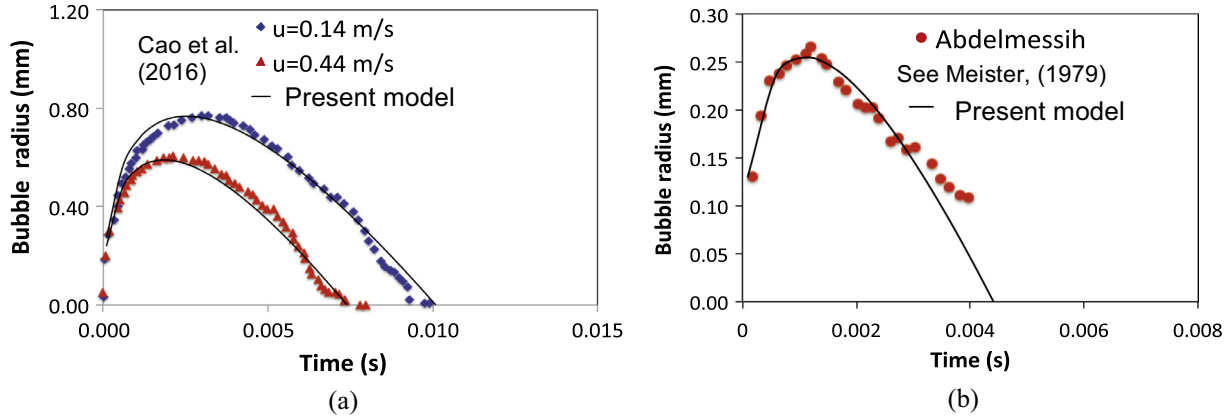

Fig. 16. Comparison of experiment and model predictions for flow boiling (a) Low subcooling- Low Velocity (LS-LV) condition (b) Low Subcooling-Medium Velocity (LS-MV) condition.

Table 10
Comparison of bubble radius for Unal's [48] experiment with model prediction.

Pressure (bar)	Wall superheat (K)	Subcooling (K)	Velocity (m/s)	Experimental R (mm)	Predicted R (mm)	% Deviation
139	3.5	3.7	3.27	0.075	0.077	+2.67
139	3.7	4.3	3.27	0.070	0.071	+1.43
139	3.9	3.7	3.27	0.090	0.089	−1.11
139	3.5	5.9	3.27	0.055	0.054	−1.82
158	4.2	4.1	3.57	0.075	0.078	+4.00
177	5.2	3.0	3.75	0.065	0.067	+3.08

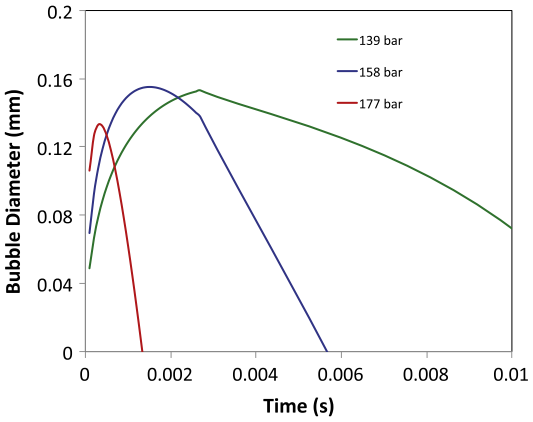

Fig. 17. Predicted bubble growth rate trend for high pressures and operating conditions of Unal [48] (Comparison against the maximum bubble radius of Unal [48] is presented in Table 10.

To test the model's ability to predict bubble growth at high velocities and low subcooling conditions, high-pressure data of Unal [48] was chosen. However, Unal's results are only in terms of the maximum diameter reached by the growing bubble. The maximum radius predicted by the present model is compared against the experimental values of Unal [48] in Table 10. For the pressures mentioned in these experiments, bubble diameter growth with time is expected to follow the trend shown in Fig. 17. As expected, at higher pressures, the bubble condenses earlier.

4.2.2. Flow boiling: high subcooling

Cao et al. [7] have also performed experiments for high subcooling conditions. Bubble growth rate predictions from the present model are compared against their experimental data in Fig. 18(a). For slightly increased velocities, the bubble growth experiments of Prodonavic et al. (2002) was employed for comparison as shown in Fig. 18(b) for 3 bar pressure. In both cases, good predictions can be noticed.

The experimental investigations of Mayinger and Bucher (see Ref. [28]) at medium velocities and a pressure of 2.05 bar were used for comparison for medium velocity and high subcooling conditions. The flow boiling wall-bubble growth model is able to predict growth in a square duct considerably well depicted in Fig. 19 (a).

Gunther's data (see Ref. [28]) available for high velocity conditions and at pressures of 1.7 bar, is used for comparison against the present model (Fig. 19(b)). The bubble growth predictions have a good agreement between the two.

In summary, it can be noticed that, for flow boiling under both low and high subcooling over a range of velocities (low, medium, high) good bubble growth rate predictions could be noticed. Based on the aforementioned comparisons for flow boiling conditions, the range of values for n_1 and n_2 employed in the model are summarized in Table 11.

5. Summary

In this study, a new generalized bubble growth model for water is proposed. The present formulation generalizes a wide range of operating conditions: pressure range of 1–180 bar, pool and flow boiling conditions, vertical and horizontal test section orientation, low and high subcooling, etc. The framework of bubble growth model is structured and parameterized so as to enable easy implementation into the Eulerian-Eulerian Multiphase Flow solvers. This would in turn help the design of high-pressure industrial systems by accurately predicting the heat transfer coefficient. The predictive capability of the model is found to be in good agreement with the experimental data.

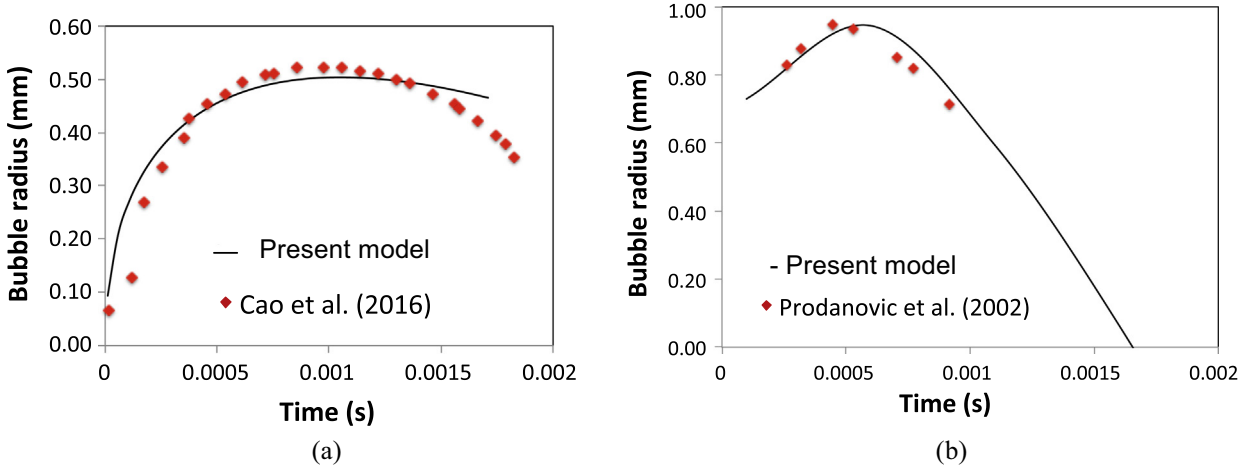

Fig. 18. Bubble growth rate predictions for flow boiling at High subcooling- Low Velocity (HS-LV) condition against (a) Cao et al. [7] (b) Prodanovic et al. [36]

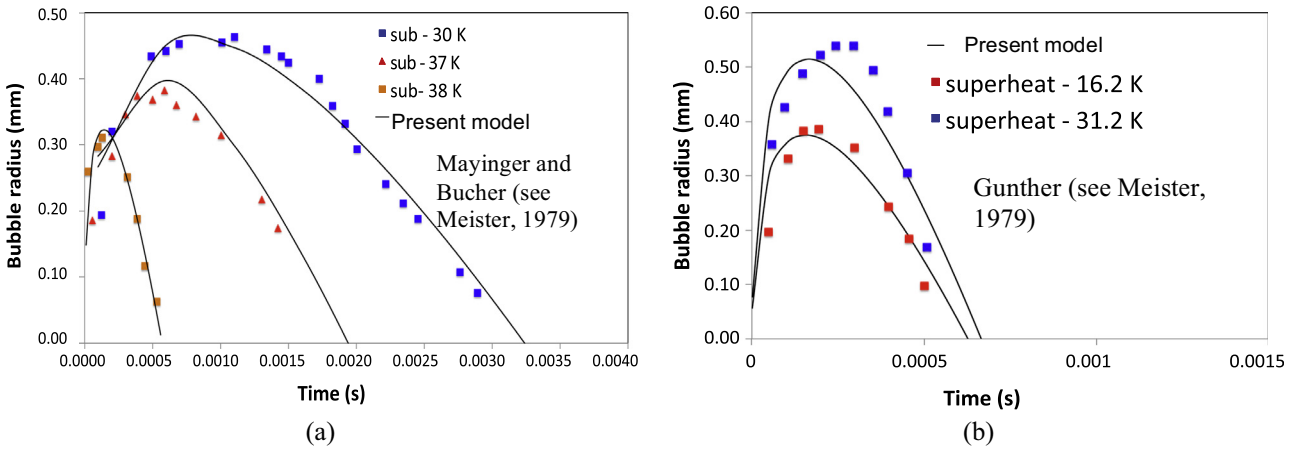

Fig. 19. Comparison of experiment and model predictions for flow boiling at (a) High subcooling- medium Velocity (HS-MV) condition (a) High subcooling- High Velocity (HS-HV) condition.

Table 11
Range of values for n_1 and n_2 used in Eqs. (6) and (9).

	ΔT_{sub} (K)	u (m/s)	n_1	n_2
Low subcooling-low velocity (LSLV)	<10	<1	0.05–0.1	0.8–0.95
Low subcooling-medium velocity (LSMV)	<10	1 < u < 3	0.05	1.05
Low subcooling-high velocity (LSHV)	<10	>3	0.3–0.5	0.1–0.5
High subcooling-low velocity (HSLV)	>10	<1	0.2–0.5	0.3–0.4
High subcooling-medium velocity (HSMV)	>10	1 < u < 3	0.05–0.15	0.35–0.45
High subcooling-high velocity (HSHV)	>10	>3	0.25–0.35	0.15–0.20

The present bubble growth model has shown that, with increase in pressure, the bubble growth rate decreases, for both pool and flow boiling conditions. Additionally, the growth rate for vertical pool boiling conditions is observed to be greater than the horizontal pool boiling condition. However, it is interesting to notice that, bubble growth decreases for higher pressures. For subcooled conditions, the bubbles are observed to grow to a maximum size attainable was found to decrease. With increase in pressure, the maximum size attainable was found to decrease. Additionally, the rate of collapse of the bubble also increased with increase in pressure.

The wake effect at the apex of a bubble growing under pool boiling conditions was found to influence the overall bubble growth rate. Similarly under flow boiling conditions, the base and apex thermal layer distortion factors were modeled for an accurate bubble growth prediction.

Conflict of interest

None declared.

Acknowledgements

The authors sincerely thank the anonymous referees for their valuable comments and suggestions. The authors acknowledge consistent support from the Board of Research in Nuclear Sudies (BRNS), Deparmtent of Atomic Energy (DAE), Government of India.

Appendix A. Supplementary material

Supplementary data associated with this article can be found, in the online version, at https://doi.org/10.1016/j.ijheatmasstransfer.2018.01.070.

References

[1] M. Akiyama, F. Tachibana, N. Ogawa, Effect of pressure on bubble growth in pool boiling, Bull. Jap. Soc. Mech. Eng. 12 (53) (1969) 1121–1128.
[2] C.N. Ammerman, Y.S. Hong, S.M. You, Identification of pool boiling heat transfer mechanisms from a wire immersed in saturated FC-72 using a single photo/LDA method, ASME J. Heat Transf. 118 (1996) l l7.
[3] S. Bae, M.H. Kim, J. Kim, Improved technique to measure time and space resolved heat transfer under single bubbles during saturated pool boiling of FC-72, Exp. Heat Transf. 12 (3) (1999) 265–278.
[4] J.D. Benardin, I. Mudawar, C.B. Walsh, E.I. Franses, Contact angle temperature dependence for water droplets on practical aluminium surfaces, Int. J. Heat Mass Transf. 40 (5) (1997) 1017–1033.
[5] L. Biasi, P. Stipari, A. Tozzi, Bubble growth in non-uniform temperature fields, Chem. Eng. Sci. 26 (1971) 867–873.
[6] S.J. Board, R.B. Duffey, Spherical vapour bubble growth in superheated liquids, Chem. Eng. Sci. 26 (1971) 263–274.
[7] Y. Cao, Z. Kawara, T. Yokomine, T. Kunugi, Visualization study on bubble dynamical behavior in subcooled flow boiling under various subcooling degree and flowrates, Int. J. Heat Mass Transf. 93 (2016) 839–852.
[8] Z. Chen, A. Haginiwa, Y. Utaka, Detailed structure of microlayer in nucleate pool boiling for water measured by laser interferometric method, Int. J. Heat Mass Transf. 108 (Part B) (2017) 1285–1291.
[9] R. Cole, H.L. Shulman, Bubble growth rates at high jakob numbers, Int. J. Heat Mass Transf. 9 (1966) 1377–1390.
[10] M. Colombo, M. Fairweather, Prediction of bubble departure in forced convection boiling: a mechanistic model, Int. J. Heat Mass Transf. 85 (2015) 135–146.
[11] M.G. Cooper, A.J.P. Lloyd, The microlayer in nucleate pool boiling, Int. J. Heat Mass Transf. 12 (8) (1969) 895–913.
[12] R. Darby, The dynamics of vapor bubbles in nucleate boiling, Chem. Eng. Sci. 19 (1964) 39–49.
[13] P. Dergarabedian, The rate of growth of vapor bubbles in superheated water, J. Appl. Mech. 20 (4) (1953) 537–545.
[14] O.E. Dwyer, Growth rates of hemispherical bubbles in nucleate boiling of liquid metals, Chem. Eng. Sci. 31 (1976) 187–193.
[15] C.E. Faneuff, E.A. McLean, V.E. Scherrer, Some aspects of surface boiling, J. Appl. Phys. 29 (8) (1958) 80–84.
[16] H.K. Forster, N. Zuber, Growth of a vapor bubble in a superheated liquid, J. Appl. Phys. 25 (1954) 474.
[17] P. Griffith, Bubble Growth Rates in Boiling, Technical Report No. 8., Grant Number NSFG-1706, 1956, pp. 1–38.
[18] C.-Y. Han, P. Griffith, The Mechanism of Heat Transfer in Nucleate Pool Boiling, MIT Technical Report No. 7673-19, 1962.

[19] R.L. Judd, K.S. Hwang, A comprehensive model for nucleate pool boiling heat transfer including microlayer evaporation, ASME. J. Heat Transf. 98 (4) (1976) 623–629.
[20] S. Jung, H. Kim, An experimental study on heat transfer mechanisms in the microlayer using integrated total reflection. laser interferometry and infrared thermometry technique, Heat Trans. Eng. 36 (2015) 1002–1012.
[21] J. Kim, B.D. Oh, M.H. Kim, Experimental study of pool temperature effects on nucleate pool boiling, Int. J. Multiph. Flow 32 (2006) 208–231.
[22] P.G. Kosky, Bubble growth measurements in uniformly superheated liquids, Chem. Eng. Sci. 23 (1968) 695–706.
[23] H.S. Lee, H. Merte Jr., Spherical vapor bubble growth in uniformly superheated liquids, Int. J. Heat Mass Transf. 39 (12) (1996) 2427–2447.
[24] F.J. Lesage, J.S. Cotton, A.J. Robnson, Modeling of quasi-static adiabatic bubble formation, growth and detachment for low Bond numbers, Chem. Eng. Sci. 104 (2013) 742–754.
[25] F.J. Lesage, S. Siedel, J.S. Cotton, A.J. Robinson, A mathematical model for predicting bubble growth for low Bond and Jakob number nucleate boiling, Chem. Eng. Sci. 112 (2014) 35–46.
[26] O. Miyatake, I. Tanaka, N. Lior, A simple universal equation for bubble growth in pure liquids and binary solutions with a non-volatile solute, Int. J. Heat Mass Transf. 40 (1997) 1577–1584.
[27] R. Mei, W. Chen, J.F. Klausner, Vapor bubble growth in heterogeneous boiling – I. Formulation, Int. J. Heat Mass Transf. 38 (1995) 909–919.
[28] G. Meister, Vapour bubble growth and recondensation in subcooled boiling flow, Nucl. Eng. Des. 54 (1979) 97–114.
[29] B.B. Mikic, W.M. Rohsenow, P. Griffith, On bubble growth rates, Int. J. Heat Mass Transf. 13 (1970) 657–666.
[30] S. Moghaddam, K. Kiger, Physical mechanisms of heat transfer during single bubble nucleate boiling of FC-72 under saturation conditions-I. Experimental investigation, Int. J. Heat Mass Transf. 52 (5–6) (2009) 1284–1294.
[31] A. Mukherjee, V.K. Dhir, Study of lateral merger of vapor bubbles during nucleate pool boiling, J. Heat Transf. 126 (2004) 1023–1039.
[32] A. Mukherjee, S.G. Kandlikar, Numerical study of effect of contact angle on bubble growth and wall heat transfer during flow boiling of water in a microchannel, in: Annals of the Assembly for International Heat Transfer Conference, 2006, p. 13.
[33] J.S. Murallidharan, B.V.S.S.S. Prasad, B.S.V. Patnaik, G.F. Hewitt, V. Badalassi, CFD investigation and assessment of wall heat flux partitioning model for the prediction of high pressure subcooled flow boiling, Int. J. Heat Mass Transf. 103 (2016) 211–230.
[34] J.S. Murallidharan, B.V.S.S.S. Prasad, B.S.V. Patnaik, A mechanistic model for embryo size prediction at boiling incipience: 'work of formation' based approach, Int. J. Heat Mass Transf. 110 (2017) 921–939.
[35] M.S. Plesset, S.A. Zwick, The growth of vapor bubbles in superheated liquids, J. Appl. Phys. 25 (1954) 493–500.
[36] V. Prodanovic, D. Fraser, M. Salcudean, Bubble behavior in subcooled flow boiling of water at low pressures and low flow rates, Int. J. Multiph. Flow 28 (2002) 1–19.
[37] S. Raj, M. Pathak, K. Khan, An analytical model for predicting growth rate and departure diameter of a bubble in subcooled flow boiling, Int. J. Heat Mass Transf. 109 (2017) 470–481.
[38] N. Ramanujapu, Study of Growth Rate, Departure Frequency and Shape of a Single Bubble During Saturated and Subcooled Nuclear Boiling, University of California, Los Angeles, Los Angeles, CA, 1999 (Ph.D. prospectus).
[39] L. Rayleigh, On the pressure developed in a liquid during the collapse of a spherical cavity, Philos. Magaz. Ser. 6 (34) (1919) 94–98.
[40] M. Saddy, G.J. Jameson, Prediction of departure diameter and bubble frequency in nucleate boiling in uniformly superheated liquids, Int. J. Heat Mass Transf. 14 (1971) 1771–1783.
[41] H. Sakashita, Bubble growth rates and nucleation site densities in saturated pool boiling of water at high pressures, J. Nucl. Sci. Technol. 48 (5) (2011) 734–743.
[42] L.E. Scriven, On the dynamics of phase growth, Chem. Eng. Sci. 10 (1/2) (1959) 1–13.
[43] V. Sernas, F.C. Hooper, The initial vapor bubble growth on a heated wall during nucleate boiling, Int. J. Heat Mass Transf. 12 (1969) 1627–1639.
[44] P.C. Slooten, Departure of Vapor- and Gas-Bubbles in a Wide Pressure Range, Ph.D. Dissertation, 1984.
[45] P. Stephan, T. Fuchs, Local heat flow and temperature fluctuations in wall and fluid in nucleate boiling systems, Heat Mass Transf. 45 (2009) 919–928.
[46] R.M. Sugrue, The effects of orientation angle, subcooling, heat flux, mass flux, and pressure on bubble growth and detachment in subcooled flow boiling, MSc Thesis, MIT, 2012.
[47] T. Theofanous, L. Biasi, H.S. Isbin, H. Fauske, A theoretical study on bubble growth in constant and time-dependent pressure field, Chem. Eng. Sci. 24 (1969) 885–897.
[48] H.C. Unal, Maximum bubble diameter, maximum bubble-growth time and bubble-growth rate during the subcooled nucleate flow boiling of water up to 17.7 MN/m^2, Int. J. Heat Mass Transf. 19 (1976) 643–649.
[49] Y. Utaka, Y. Kashiwabara, M. Ozaki, Microlayer structure in nucleate boiling of water and ethanol at atmospheric pressure, Int. J. Heat Mass Transf. 57 (2013) 222–230.
[50] Y. Utaka, Y. Kashiwabara, M. Ozaki, Z. Chen, Heat transfer characteristics based on microlayer structure in nucleate pool boiling for water and ethanol, Int. J. Heat Mass Transf. 68 (2014) 479–488.
[51] S.J.D. Van Stralen, The growth rate of vapour bubbles in superheated pure liquids and binary mixtures part II: experimental results, Int. J. Heat Mass Transf. 11 (1967) 1491–1512.
[52] S.J.D. van Stralen, The growth rate of vapour bubbles in superheated pure liquids and binary mixtures part I: theory, Int. J. Heat Mass Transf. 11 (1968) 1467–1489.
[53] S.J.D. Van Stralen, M.S. Sohal, R. Cole, W.M. Sluyter, Bubble growth rates in pure and binary systems: combined effect of relaxation and evaporation microlayers, Int. J. Heat Mass Transf. 18 (1975) 453–467.
[54] J. Wu, V.K. Dhir, Numerical simulations of dynamics and heat transfer associated with a single bubble in subcooled pool boiling, J. Heat Transf. 132 (111501) (2010) 1–15.
[55] T. Yabuki, T. Hamaguchi, O. Nakabeppu, Interferometric measurement of the liquid-phase temperature field around an isolated boiling bubble, J. Therm. Sci. Tech. 7 (3) (2012) 463–474.
[56] T. Yabuki, O. Nakabeppu, Heat transfer mechanisms in isolated bubble boiling of water observed with MEMS sensor, Int. J. Heat Mass Transf. 76 (2014) 286–297.
[57] T. Yabuki, O. Nakabeppu, Microscale wall heat transfer and bubble growth in single bubble subcooled boiling of water, Int. J. Heat Mass Transf. 100 (2016) 851–860.
[58] G.H. Yeoh, C.P. Sherman, T.Y. Tu, Mark K.M. Ho, Fundamental consideration of wall heat partition of vertical subcooled boiling flows, Int. J. Heat Mass Transf 51 (15–16) (2008) 3840–3853.
[59] B.J. Yun, A. Splawski, S. Lo, C.-H. Song, Prediction of a subcooled boiling flow with advanced two-phase flow models, Nucl. Eng. Des. 253 (2011) 351–359.
[60] N. Zuber, The dynamics of vapor bubbles in non-uniform temperature fields, Int. J. Heat Mass Transf. 2 (1961) 83–98.